

# metaDMG – An Ancient DNA Damage

## 2 Toolkit

✉ For correspondence:

christianmichelsen@gmail.com

(CM); [mwpedersen@sund.ku.dk](mailto:mwpedersen@sund.ku.dk)

(MW);

[tskorneliussen@sund.ku.dk](mailto:tskorneliussen@sund.ku.dk)

(TSK).

<sup>†</sup>Authors contributed equally.

**Present address:** Niels Bohr Institute, University of Copenhagen, Blegdamsvej 17, 2100 Copenhagen, Denmark.

**Data availability:** The source code for metaDMG is available on [Zenodo](#) or at the [Github](#) repository. All code used in the statistical analysis can be found at the following DOI: [10.5281/zenodo.7368194](https://doi.org/10.5281/zenodo.7368194).

Sequencing data and supporting material used in simulations can be found at [ERDA](#).

**Funding:** CM and TP is funded by the Lundbeck Foundation. MWP is funded by the ERC project LASTJOURNEY (ERC\_Adv\_834514). TSK is funded by Carlsberg grant CF19-0712.

**Competing interests:** The author declare no competing interests.

Christian Michelsen<sup>1,2</sup> <sup>†</sup> , Mikkel Winther Pedersen<sup>2</sup> <sup>†</sup> , Antonio

4 Fernandez-Guerra<sup>2</sup> , Lei Zhao<sup>2</sup>, Troels C. Petersen<sup>1</sup> , Thorfinn Sand Korneliussen<sup>2</sup>

6 <sup>1</sup>Niels Bohr Institute, University of Copenhagen

2Globe Institute, University of Copenhagen

8

---

## Abstract

10 **1. Motivation** Under favourable conditions DNA molecules can persist for hundreds of thousands of years (Valk et al., 2021; Zavala et al., 2021). Such genetic remains make up invaluable resources to study past assemblages, populations, and even the evolution of species. However, DNA is subject to enzymatic, chemical, and mechanical degradation, and hence over time decrease to ultra low concentrations which makes it highly prone to contamination by modern sources that are rich in DNA. Strict precautions and criteria (Gilbert et al., 2005; Champlot et al., 2010; Llamas et al., 2017) are therefore necessary to ensure that DNA from modern sources does not appear in the final data and that the taxa is authenticated as ancient. The most generally accepted and widely applied authenticity for ancient DNA studies is to test for elevated deaminated cytosine residues towards the termini of the molecules: DNA damage (Briggs et al., 2007; Dabney, Meyer, and Pääbo, 2013). To date, this has primarily been used for single organisms (Jónsson et al., 2013) and recently for read assemblies (Borry et al., 2021), however, these methods have not been designed, nor are they computationally up-scalable, for estimating DNA damage for ancient metagenomes with tens and even hundreds of thousands of species.

24 **2. Methods** We present metaDMG, a novel framework that takes advantage of the information already contained within standard alignment files to compute and statistically evaluate

misincorporations due to DNA damage. It thus bypasses any need for initial classification,  
28 splitting reads by individual organisms, realigning these to the reference genome and lastly  
parse alignments to mapDamage2.0 (Jónsson et al., 2013). We have implemented a  
30 Bayesian approach that combines a modified geometric damage profile with a  
beta-binomial model to fit the entire model to the individual misincorporations at all  
32 taxonomic levels. metaDMG was hereafter benchmarked using sets of simulated data of single  
genomes and metagenomes. Lastly, it was tested on published datasets and its  
34 performance compared to existing methods.

3. **Results** We find metaDMG to be an order of magnitude faster than previous methods and  
36 more accurate – even for complex metagenomes with tens of thousands of species. Our  
simulations show that metaDMG can estimate DNA damage at taxonomic levels down to 100  
38 reads, that the estimated uncertainties decrease with increased number of reads and that  
the estimates are more significant with increased number of C to T misincorporations.

40 4. **Conclusion** metaDMG is a state-of-the-art program for ancient DNA damage estimation and  
further allows for the computation of nucleotide misincorporation, GC-content, and DNA  
42 fragmentation for both simple and complex ancient genomic datasets. Finally, also it  
includes the PMDtools statistics (Skoglund et al., 2014) that allow for the extraction of  
44 individual reads with ancient damage, making it a complete package for ancient DNA  
damage authentication.

46 **keywords:** ancient DNA, DNA damage estimation, DNA damage, metaDMG, metagenomics.

---

## 48 1 | INTRODUCTION

Throughout the life of an organism it contaminates its environment with DNA, cells, or tissue, thus  
50 leaving genetic traces behind. As the cell leaves its host, DNA repair mechanisms stops and the DNA  
is subjected to intra and extra cellular enzymatic, chemical, and mechanical degradation, resulting  
52 in fragmentation and molecular alterations that over time lead to the characteristics of ancient  
DNA (Briggs et al., 2007; Dabney, Meyer, and Pääbo, 2013). Ancient DNA (aDNA) has been shown  
54 to persist in a diverse variety of environmental contexts, e.g. within fossils such as bones, soft-  
tissue, and hair, as well as in geological sediments, archaeological layers, ice-cores, permafrost soil

56 for hundreds of thousands of years (Valk et al., 2021; Zavala et al., 2021). Common for all is that  
they have an accumulated amount of deaminated cytosines towards the termini of the DNA strand,  
58 which, when amplified, results in misincorporations of thymines on the cytosines (Ginolhac et al.,  
2011; Dabney, Meyer, and Pääbo, 2013).

60 Even though postmortem DNA damage (PMD) is characterized by the four Briggs parameters  
(Briggs et al., 2007), they are rarely used directly for asserting “ancientness”. Researchers work-  
62 ing with ancient DNA tend to simply use the empirical C→T on the first position of the fragment  
together with other supporting summary statistic of the experiment (Jónsson et al., 2013). Quantify-  
64 ing PMD have become standard for single individual sources like hair, bones, teeth and also ap-  
plied to smaller subsets of species in ancient environmental metagenomes (Pedersen et al., 2016;  
66 Murchie et al., 2021; Wang, Pedersen, et al., 2021; Zavala et al., 2021). While this is a relatively fast  
process for single individuals it becomes increasingly demanding, iterative, and time consuming as  
68 the samples and the diversity within increases, as in the case for metagenomes from ancient soil,  
sediments, dental calculus, coprolites, and other ancient environmental sources. It has therefore  
70 been practice to estimate damage for only the key taxa of interest in a metagenome, as metage-  
nomic samples easily include tens of thousands of different taxonomic entities, which makes a  
72 complete estimate across the metagenomes computationally intractable, if not an impossible task  
(Pedersen et al., 2016). To overcome these limitations, we designed a toolkit called `metaDMG` (pro-  
74 nounced metadamage) which allows for the rapid computation of various statistics relevant for the  
quantification of PMD at read level, single genome level, and even metagenomic level by taking into  
76 account the intricate branching structure of the taxonomy of the possible multiple alignments for  
the single reads.

78 Our thorough analysis with both simulated and real data shows that `metaDMG` is both faster at  
ancient DNA damage estimation and provides more accurate damage estimates. Furthermore, as  
80 `metaDMG` is designed with the increasingly large datasets that are currently generated in the field  
of ancient environmental DNA in mind, `metaDMG` is able to process complex metagenomes within  
82 hours instead of days. At the same time, it outperforms standard tools that estimate DNA damage  
for single genomes and samples with low complexity. Furthermore, it can compute a global dam-  
84 age estimate for a metagenome as a whole. Lastly, `metaDMG` is compatible with the NCBI taxonomy  
and use `ngsLCA` (Wang, T. S. Korneliussen, et al., 2022) to perform a lowest common ancestor (LCA)  
86 classification of the aligned reads to get precise damage estimates at all taxonomic levels. It also

allows for custom taxonomies and thus also the use of metagenomic assembled genomes (MAGs)  
88 as references.

This paper is organized as follows. In *section 2* we present our statistical models including two  
90 novel test statistics,  $D_{\text{fit}}$  and  $Z_{\text{fit}}$ . We quantify the performance of our test statistics using various  
simulation approaches in *section 3*. The results of these simulations is shown in *section 4* and  
92 finally, the method and results are discussed in *section 5*.

## 2 | METHODS & MATERIALS

94 To quantify ancient damage, one can either compute it on a per read level or across an entire  
taxa. A priori, the actual biochemical changes which characterizes post mortem damage in a  
96 single read cannot be directly observed, but by aligning each fragment and considering the ob-  
served difference between the reference and read, the possible PMD can be computed. We have  
98 (re)implemented the approach used in PMDtools (Skoglund et al., 2014) which allows for the ex-  
traction of single DNA reads which are estimated to contain PMD, see *Appendix 1*. This approach,  
100 will preferentially choose reads that has excess of C→T in the first positions and can not be used  
directly for asserting or quantifying to what degree a given library might contain damaged frag-  
102 ments. We have therefore developed a novel statistical method that aims to mitigate this caveat  
by using all reads or reads that aligns to specific taxa. First we will define the mismatch matrices  
104 in *subsection 2.1* followed by the lowest common ancestor method in *subsection 2.2*. The mis-  
match matrices can further be improved by multinomial regression, see *subsection 2.3*, however,  
106 this requires more data than than what is usually available in metagenomic studies. As such, we  
present the beta-binomial damage model in *subsection 2.4* which aims to work even on extremely  
108 low-coverage data.

### 2.1 | Mismatch matrices/nucleotide misincorporation patterns

110 We seek to obtain the pattern or signal of damage across multiple reads by generating what is  
called the mismatch matrix or the nucleotide misincorporation matrix. This matrix represents  
112 the nucleotide substitution counts across reads and provides us with the position dependent mis-  
match matrices,  $M(x)$ , with  $x$  denoting the position in the read, starting from 1. At a specific position  
114  $x$ ,  $M_{\text{ref} \rightarrow \text{obs}}(x)$  describes the number of nucleotides that was mapped to a reference base  $B_{\text{ref}}$  but  
was observed to be  $B_{\text{obs}}$ , where  $B$  is one of the four bases: A, C, G, T. The number of C→T transitions

116 at the first position, e.g., is denoted as  $M_{C \rightarrow T}(x = 1)$ .

Entire reads can be discarded based on low mapping quality, and single nucleotides similarly  
118 if the base quality score fall below some threshold. The quality scores could also be used as probabilistic weights, however, due to the four-bin discretization of quality scores on modern day sequencing machines, we limit the use of these to filtering.  
120

## 2.2 | Lowest Common Ancestor and Mismatch matrices

122 For environmental DNA (eDNA) studies a competitive alignment approach is routinely applied. Here all possible alignments for a given read are considered. Each read is mapped against a multi  
124 species reference databases (e.g. nucleotide or RefSeq from NCBI or custom downloaded). A single read might map to a highly conserved gene that is shared across higher taxonomic ranks such  
126 as class or even domains. This read will not provide relevant information due to the generality, whereas a read that maps solely to a single species or species from a genus would be indicative of  
128 the read being well classified. We limit the tabulation and construction of the mismatch matrices to the subset of reads that are well classified.

130 For each read, we compute the lowest common ancestor using all alignments contained within the user defined taxonomic threshold (species, genus or family) and tabulate the mismatches matrices for each cycle (Wang, T. S. Korneliussen, et al., 2022). If none of the alignments pass the filtering thresholds (excess similarity, mapping quality, etc.), the read is discarded. Depending on  
132 the run mode, we allow for the construction of these mismatch matrices on three different levels.

134 Firstly, we can obtain a basic single global mismatch matrix which could be relevant in a standard single genome aDNA study and similar to the tabulation used in mapDamage (Jónsson et al., 2013).

136 Secondly, we can obtain the per reference counts, or, finally, if a taxonomy database has been supplied, we can build mismatch matrices at the species level and aggregate from leaf nodes to the internal taxonomic ranks (genus, kingdom etc) towards the root. We will use the term “taxa”  
138 to refer to either of these levels; i.e. a specific taxa can either refer to a specific LCA, a specific reference, or all reads in a global estimate, depending on the run-mode.

140 When aggregating the mismatch matrices for the internal nodes in our taxonomic tree, two different approaches can be taken. Either all alignments of the read will be counted, which we will  
142 refer to as weight-type 0, or the counts will be normalized by the number of alignments of each read; weight-type 1, which is the default.

## <sup>146</sup> 2.3 | Regression Framework

The nucleotide misincorporation frequencies are routinely used as the basis for assessing whether or not a given library is ancient by looking at the expected drop of C→T (or its complementary G→A) frequencies as a function of the position of the reads. This signal is caused by a higher deamination rate in the single-strand part of the damaged fragment than that in the double strand part. The mismatch matrix is constructed based on the empirical observations and are subject to stochastic noise. The effect of noise in the mismatch matrix can be limited by the use of the multinomial regression model. We continue the work of Cabanski et al., 2012 to provide four different regression methods to stabilize the raw mismatch matrix across all combinations of reference bases, observed bases, strands and positions, see *Appendix 2* for details, derivation and results. Given enough sequencing data, this approach will provide an improved, noise-reduced mismatch matrix which would be relevant for single genome ancient DNA studies. However, for extremely low coverage studies, such as environmental DNA, the method is likely to overfit and would not be as suitable as the simplified model described in the *subsection 2.4*.

## <sup>160</sup> 2.4 | Damage Estimation

In standard ancient DNA context it is generally not possible to obtain vast amounts of data and thus we propose two novel tests statistics,  $D_{\text{fit}}$  and  $Z_{\text{fit}}$ , that are especially suited for this common scenario. The damage pattern observed in aDNA has several features which are well characterized. By modelling these, one can construct observables sensitive to aDNA signal. We model the damage patterns seen in ancient DNA by looking exclusively at the C→T transitions in the forward direction (5') and the G→A transitions in the reverse direction (3'). For each taxa, we denote the number of transitions,  $k(x)$ , as:

$$\begin{aligned} \text{168} \quad k(x) = & \begin{cases} M_{C \rightarrow T}(x) & \text{for } x > 0 \quad (\text{forward}) \\ M_{G \rightarrow A}(x) & \text{for } x < 0 \quad (\text{reverse}), \end{cases} \end{aligned} \quad (1)$$

<sup>170</sup> and the number of reference counts  $N(x)$ :

$$\begin{aligned} \text{172} \quad N(x) = & \begin{cases} \sum_{i \in \{A,C,G,T\}} M_{C \rightarrow i}(x) & \text{for } x > 0 \quad (\text{forward}) \\ \sum_{i \in \{A,C,G,T\}} M_{G \rightarrow i}(x) & \text{for } x < 0 \quad (\text{reverse}). \end{cases} \end{aligned} \quad (2)$$

The damage frequency is thus  $f(x) = k(x)/N(x)$ .

<sup>174</sup> A natural choice of likelihood model would be the binomial distribution. However, we found  
<sup>175</sup> that a binomial likelihood lacks the flexibility needed to deal with the large amount of variance  
<sup>176</sup> (overdispersion) we found in the data due to poorly curated references and possible misalignments.

To accommodate overdispersion, we instead apply a beta-binomial distribution,  $\mathcal{P}_{\text{BetaBinomial}}$ , which  
<sup>178</sup> treats the probability of deamination,  $p$ , as a random variable following a beta distribution<sup>1</sup> with  
<sup>179</sup> mean  $\mu$  and concentration  $\phi$ :  $p \sim \text{Beta}(\mu, \phi)$ . The beta-binomial distribution has the following  
<sup>180</sup> probability density function:

$$\mathcal{P}_{\text{BetaBinomial}}(k | N, \mu, \phi) = \binom{N}{k} \frac{B(k + \mu\phi, N - k + \phi(1 - \mu))}{B(\mu\phi, \phi(1 - \mu))}, \quad (3)$$

<sup>1</sup> Note that we do not parameterize the beta distribution in terms of the common  $(\alpha, \beta)$  parameterization, but instead using the more intuitive  $(\mu, \phi)$  parameterization. One can re-parameterize  $(\alpha, \beta) \rightarrow (\mu, \phi)$  using the following two equations:  $\mu = \frac{\alpha}{\alpha+\beta}$  and  $\phi = \alpha + \beta$  (Cepeda-Cuervo and Cifuentes-Amado, 2017).

where  $B$  is defined as the beta function:

$$B(x, y) = \frac{\Gamma(x)\Gamma(y)}{\Gamma(x+y)}, \quad (4)$$

<sup>182</sup> with  $\Gamma(\cdot)$  being the gamma function (Cepeda-Cuervo and Cifuentes-Amado, 2017).

The close resemblance to a binomial model is most easily seen by comparing the mean and  
<sup>188</sup> variance of a random variable  $k$  following a beta-binomial distribution,  $k \sim \mathcal{P}_{\text{BetaBinomial}}(N, \mu, \phi)$ :

$$\begin{aligned} \mathbb{E}[k] &= N\mu \\ \mathbb{V}[k] &= N\mu(1-\mu)\frac{\phi+N}{\phi+1}. \end{aligned} \quad (5)$$

<sup>190</sup> The expected value of  $k$  is similar to that of a binomial distribution and the variance of the beta-binomial distribution reduces to a binomial distribution as  $\phi \rightarrow \infty$ . The beta-binomial distribution  
<sup>191</sup> can thus be seen as a generalization of the binomial distribution.

Note that both equation (3) and (5) relate to the damage at a specific base position (cycle),  
<sup>194</sup> i.e. for a single  $k$  and  $N$ . To estimate the overall damage in the entire read using the position  
<sup>195</sup> dependent counts,  $k(x)$  and  $N(x)$ , we model  $\mu$  as being position dependent,  $\mu(x)$ , and assume a  
<sup>196</sup> position-independent concentration,  $\phi$ . We model the damage frequency with a modified geometric sequence, i.e. exponentially decreasing for discrete values of  $x$ :

$$y(x; A, q, c) = A(1-q)^{|x|-1} + c. \quad (6)$$

<sup>198</sup> Here  $A$  is the amplitude of the damage and  $q$  is the relative decrease of damage pr. position. A  
<sup>199</sup> background,  $c$ , was added to reflect the fact that the mismatch between the read and reference  
<sup>200</sup> might be due to other factors than just ancient damage. As such, we allow for a non-zero amount  
<sup>201</sup> of damage, even as  $x \rightarrow \infty$ . This is visualized in **Figure 1** along with a comparison between the  
<sup>202</sup> classical binomial model and the beta-binomial model.

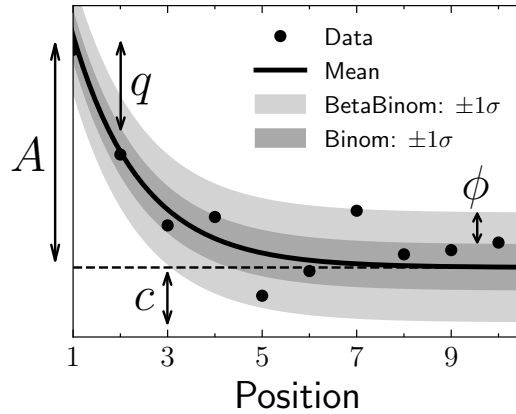


**Figure 1.** Illustration of the damage model. The figure shows data points as circles and the damage,  $f(x)$ , as a solid line. The amplitude of the damage is  $A$ , the offset is  $c$ , and the relative decrease in damage pr. position is given by  $q$ . The damage uncertainty for a binomial model is shown in dark grey and the uncertainty for a beta-binomial model in light grey.

<sup>2</sup> Parameterized as  $(\mu, \phi)$

To estimate the four fit parameters,  $A$ ,  $q$ ,  $c$ , and  $\phi$ , we apply Bayesian inference to utilize domain specific knowledge in the form of priors. We assume weakly informative beta-priors<sup>2</sup> for both  $A$ ,  $q$ , and  $c$ . In addition to this, we assume an exponential prior on  $\phi$  with the requirement of  $\phi > 2$  to avoid too much focus on 0-or-1 probabilities (McElreath, 2020). The final model is thus:

$$\begin{aligned}
 [A \text{ prior}] \quad & A \sim \text{Beta}(0.1, 10) \\
 [q \text{ prior}] \quad & q \sim \text{Beta}(0.2, 5) \\
 [c \text{ prior}] \quad & c \sim \text{Beta}(0.1, 10) \\
 [\phi \text{ prior}] \quad & \phi \sim 2 + \text{Exponential}(1/1000) \\
 [\text{likelihood}] \quad & k_i \sim \mathcal{P}_{\text{BetaBinomial}}(N_i, y(x_i; A, q, c), \phi),
 \end{aligned} \tag{7}$$

where  $i$  is an index running over all positions.

We define the damage due to deamination,  $D$ , as the background-subtracted damage frequency at the first position:  $D \equiv y(x = \pm 1) - c$ . As such,  $D$  is the damage related to ancientness. Using the properties of the beta-binomial distribution, eq. (5), we find the mean and variance of  $D$ :

$$\begin{aligned}
 \mathbb{E}[D] \equiv D_{\text{fit}} &= A \\
 \mathbb{V}[D] \equiv \sigma_D^2 &= \frac{A(1-A)}{N} \frac{\phi + N}{\phi + 1}.
 \end{aligned} \tag{8}$$

Since  $D$  estimates the overexpression of damage due to ancientness, not only is the mean of  $D$ ,  $D_{\text{fit}}$ , relevant but also the certainty of it being non-zero (and positive). We quantify this through the

222 significance  $Z_{\text{fit}} = D_{\text{fit}}/\sigma_D$  which is thus the number of standard deviations ("sigmas") away from  
223 zero. Assuming a Gaussian distribution of  $D$ ,  $Z_{\text{fit}} > 2$  would indicate a probability of  $D$  being larger  
224 than zero, i.e. containing ancient damage, with more than 97.7% probability. This assumption  
works well in the case of many reads or a high amount of damage due to central limit theorem.

226 When the assumption breaks down, the significance is still a relevant test statistic, it is only the  
conversion to a probability that will become biased.

228 These two values allows us to not only quantify the amount of ancient damage ( $D_{\text{fit}}$ ) but also the  
certainty of this damage ( $Z_{\text{fit}}$ ) without having to run multiple models and comparing these. An intu-  
230 itive interpretation of our  $D_{\text{fit}}$  statistic is, that this is the excess deamination in the beginning of the  
read, taking all cycle positions into account and excluding the constant deamination background

232 (c). This is visually similar to the  $A$  parameter in [Figure 1](#).

We perform the Bayesian inference of the parameters models using Hamiltonian Monte Carlo  
234 (HMC) sampling which is a particular of Monte Carlo Markov Chain (MCMC) algorithm (Betancourt,  
235 2018). Specifically, we use the NUTS implementation in NumPyro (Phan, Pradhan, and Jankowiak,  
236 2019), a Python package which uses JAX (Bradbury et al., 2018) under the hood for automatic differ-  
entiation and JIT compilation. We treat each taxa as being independent and generate 1000 MCMC  
238 samples after an initial 500 samples as warm up.

Since running the full Bayesian model is computationally expensive, we also allow for a faster,  
240 approximate method by fitting the maximum a posteriori probability (MAP) estimate. We use iMi-  
nuit (Dembinski et al., 2021) for the MAP optimization with Numba acceleration (Lam, Pitrou, and  
242 Seibert, 2015) for even faster run times. On a Macbook M1 Pro model from 2021, the timings for  
running the full Bayesian model is  $1.41 \pm 0.04$  s pr. fit and for the MAP it is  $4.34 \pm 0.07$  ms pr. fit,  
244 showing more than a 2 order increase in performance (around 300x) for the approximate model.

Both models allow for easy parallelisation to decrease the computation time.

## 246 2.5 | Visualisation

We provide an interactive graphical user interface (dashboard) to visualise, explore, and manip-  
248 ulate the results from the modelling phase. An interactive example of this can be found online  
(<https://metadmg.onrender.com/>). The structure of the dashboard is explained in [Figure 2](#). The dash-  
250 board allows for filtering, styling and variable selection, visualizing the mismatch matrix related to  
a specific taxa, and exporting of both fit results and plots. By filtering, we include both filtering by

252 sample, by the summary statistics of the data (e.g. requiring  $D_{\text{fit}}$  to be above a certain threshold),  
254 and even by taxonomic level (e.g. only looking at taxa that are part of the Mammalia class). We  
greatly believe that a visual overview of the fit results increase understanding of the data at hand.  
The dashboard is implemented with Plotly plots and incorporated into a Dash dashboard (Plotly,  
256 2015).

### 3 | SIMULATION STUDY

258 To determine metaDMG's performance, we performed a set of rigorous in-silica simulations to identify  
and quantify any possible biases as well the accuracy of our test statistics. Overall, the simulations  
260 can be split two groups. The first is based on a genome from a single species and is used to mea-  
sure the performance of the actual damage estimation and damage model. The second is based  
262 on synthetic ancient metagenomic datasets using the statistics and nature of a set of published  
ancient metagenomes.

#### 264 3.1 | Single-genome simulations

The first simulations follow a simple setup in which we extract reads from a set of representa-  
266 tive genomes having variable length and GC-content. We next added post-mortem damage mis-  
incorporations using NGSNGS (Henriksen, Zhao, and T. Korneliussen, 2022) a recent implemen-  
268 tation of the original Briggs model similar to Gargammel (Neukamm, Peltzer, and Nieselt, 2021) and  
lastly added sequencing errors (REFERENCE Gargamel paper). All reads are hereafter mapped us-  
270 ing Bowtie2 against each of the respective reference genomes and ancient DNA damage estimated  
the DNA damage using metaDMG. The simulations were computed with varying amount of damage  
272 added by changing the single-stranded DNA deamination,  $\delta_{\text{SS}}$  in the original Briggs model (Briggs  
et al., 2007).

3 NCBI: NC\_012920.1

274 In detail, we focused on the following genomes; *Homo Sapiens mitochondrial*<sup>3</sup>, a *Betula nana*

4 NCBI: KX703002.1

chloroplast<sup>4</sup>, and three microbial genomes (*Fusobacterium pseudoperiodonticum*<sup>5</sup>, *Neisseria cinerea*<sup>6</sup>,

5 NCBI: NZ\_CP024731.1

276 and *Actinomyces oris* strain S64C<sup>7</sup>) with the varying GC-content, low (28%), medium (37%), and high

6 NCBI: NZ\_LS483369.1

(50%) respectively. For each simulation, we performed 100 independent replications to measure

7 NCBI: GCA\_001929375.1

278 the variability of the parameter estimation and quantify the robustness of the estimates. We fur-  
ther simulated eight different sets of damage (0%, 1%, 2%, 5%, 10%, 15%, 20%, and 30% damage  
280 on position 1), all with 13 sets of different number of reads (10, 25, 50, 100, 250, 500, 1.000, 2.500,

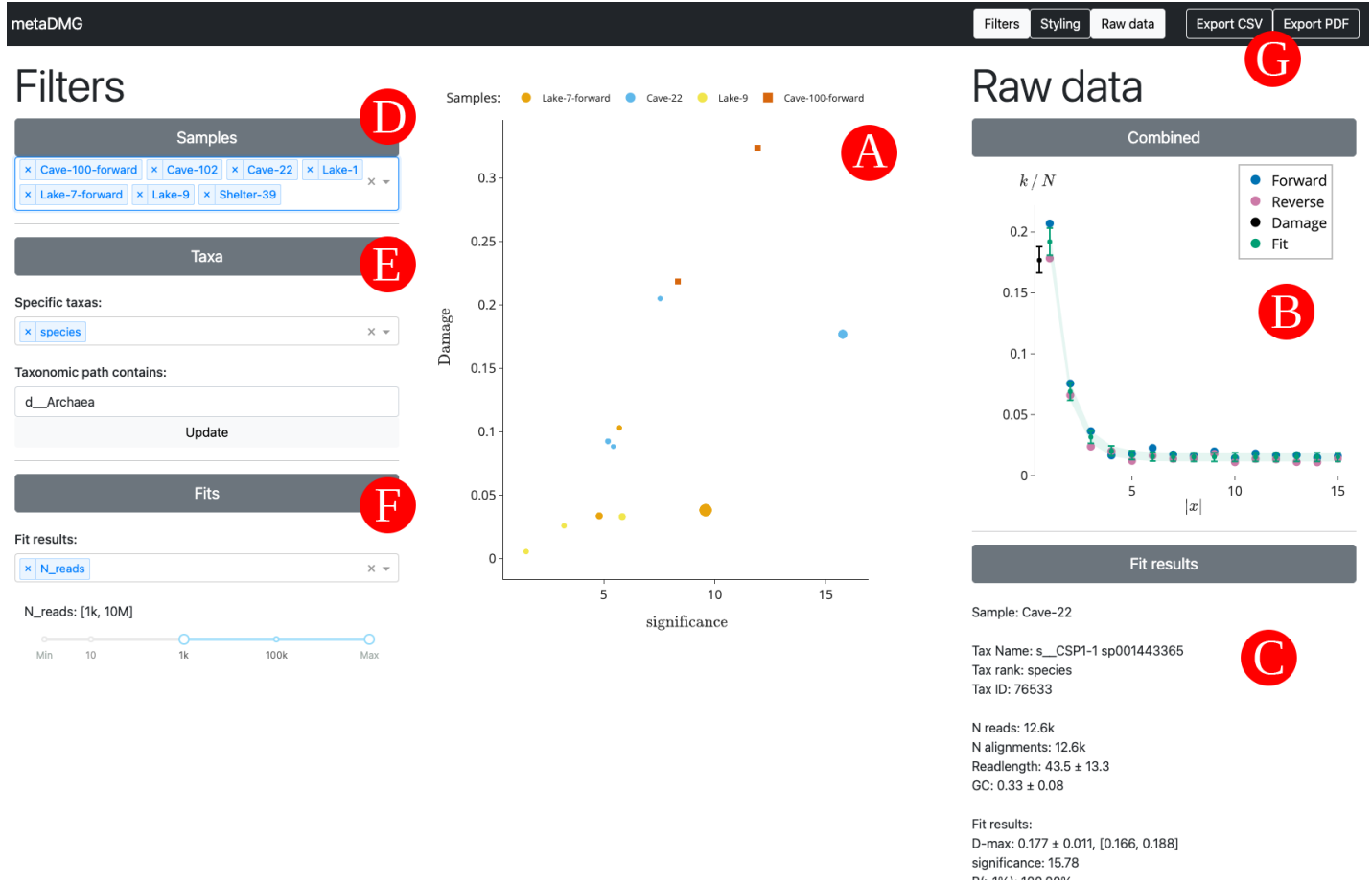


**Figure 2.** Overview of the interactive metaDMG dashboard. A) The main damage plot shows the damage ( $D_{fit}$ ) on the y-axis and the significance ( $Z_{fit}$ ) on the x-axis. Each point is a single taxa from one of the metagenomic samples, see *Table 1*. Once clicked on a specific taxa, the right-hand window shows information about the selected taxa and related fit. B) The top window shows a plot of the damage frequency for both the forward and reverse direction along with the estimated fit and damage. C) Below, the results of the fit are shown, including taxonomic information, read-specific information, the fit results, and the full taxonomic path. D) In the left filtering window, the samples to include can be selected. E) This windows allows for selection based on taxa-specific criteria. Here we show a selection of only taxa with “species” as their LCA and taxa that are part of the archaea domain. F) The final filtering window allows for setting fit related thresholds such as the minimum damage or significance. Here it is shown discarding taxa with fewer than 1000 reads. G) In the top right, after the selection and filtering process is finished, the final taxa can be exported to a CSV file along with all of the fit information, or the damage plots can be generated and saved.

5.000, 10.000, 25.000, 50.000, and 100.000 reads). We also sought to measure the effect of the  
282 fragment lengths using three sets of different fragment length distributions sampled from a *log-normal*  
normal distribution with mean 35, 60, and 90, each with a standard deviation of 10). Furthermore,  
284 to investigate whether the damage estimation by metaDMG is independent of contig size, we artifi-  
cially created three different genomes by sampling 1.000, 10.000 or 100.000 different basepairs  
286 from a uniform categorical distribution of A, C, G, and T. Based on these three genomes, we added  
artificial deamination for a different number of reads, as for the other simulations. Lastly, we also  
288 created 1000 repetitions of non-damaged simulations for Homo Sapiens to measure the rate of  
false positives. The exact commands used can be found in [Appendix 3](#).

290 To compare the damage estimates to known values, for each of the genomes mentioned above  
and for each amount of artificial damage, we generated 1.000.000 reads using NGSNGS without  
292 any added sequencing noise. The values we compare is the difference in damage frequency at  
position 1 and 15:

$$294 D_{\text{known}} = \frac{f(x=1) - f(x=15)}{2} + \frac{f(x=-1) - f(x=-15)}{2}, \quad (9)$$

which is the average of the C→T damage frequency difference and the G→A damage frequency  
296 difference.

### 3.2 | Metagenomic Simulations

298 A metagenome contains a complex mixture of organisms, all with highly different characteristics  
in GC content, read length, abundance, or degree of DNA damage, and there are large difference  
300 between and with different environments. It is therefore far from simple to obtain DNA damage  
estimates for such multitude of organisms. In order to test the accuracy and sensitivity of metaDMG,  
302 we simulated, six of the nine ancient metagenomes (with more than 1 million reads and XXX criteria)  
covering a wide span of environments and ages ([Table 1](#)).

304 First, we mapped all reads of each metagenome with bowtie2 against a database consisting of  
the GTDB (r202) (Parks et al., 2018) species cluster reference sequences, all organelles from NCBI  
306 RefSeq (NCBI Resource Coordinators, 2018), and the reference sequences from CheckV (Nayfach et  
al., 2021). We then used bam-filter v1.0.11 (Fernandez-Guerra, 2022a) with the flag --read-length-freqs  
308 to get read length distributions for each genome reads aligned to and their respective abundance.  
Next, we filtered genomes with an observed-to-expected coverage ratio greater than 0.75 using

**Table 1.** Metagenomic samples. “Name” is the name of the sample used throughout this paper. “Site” is the type of metagenomic site. “Type” is the type of environment. “Age” is the approximate age of the sample in kyr Bp. “Sediment” is the name type of sediment. “Instrument” is the Illumina model. “Library” is the library type where D. means double stranded and S. means single stranded. “Reads” is the raw number of reads (in millions). “Source” is the source of the data. The dagger (†) indicates samples that were not a part of the metagenomic simulation pipeline.

| Name                    | Site             | Type                    | Age (kyr) | Sediment         | Instrument | Library | Reads (M) | Source                       |
|-------------------------|------------------|-------------------------|-----------|------------------|------------|---------|-----------|------------------------------|
| Library-0 <sup>†</sup>  | Control          | Control                 | 0         | Reagents         | HiSeq4000  | D.      | 19.7      | (Ardelean et al., 2020)      |
| Pitch-6                 | Syltholmen pitch | Chewed organic material | 5.7       | Organic material | HiSeq2500  | D.      | 150.3     | (Jensen et al., 2019)        |
| Lake-1 <sup>†</sup>     | Spring Lake      | Lake gyttja/sediment    | 1.4       | Organic material | HiSeq 100  | D.      | 49.8      | (Pedersen et al., 2016)      |
| Lake-7                  | Lake CH12        | Lake gyttja/sediment    | 6.7       | Organic material | HiSeq2500  | S.      | 291.9     | (Schulte et al., 2021)       |
| Lake-9                  | Spring Lake      | Lake gyttja/sediment    | 9.2       | Organic material | HiSeq 100  | D.      | 128.4     | (Pedersen et al., 2016)      |
| Shelter-39 <sup>†</sup> | Abri Pataud      | Rock shelter            | 39.4      | Sediment         | MiSeq      | S.      | 0.4       | (Braadbaart et al., 2020)    |
| Cave-22                 | Chiquihuite cave | Cave sediment           | 22.2      | Carbonate rock   | HiSeq4000  | D.      | 5.7       | (Ardelean et al., 2020)      |
| Cave-100                | Eustatas Cave    | Cave sediment           | 100       | Carbonate rock   | HiSeq2500  | S.      | 21.8      | (Vernot et al., 2021)        |
| Cave-102                | Pesturina Cave   | Neanderthal tooth       | 102       | Dental calculus  | HiSeq4000  | D.      | 12.3      | (Fellows Yates et al., 2021) |

<sup>310</sup> bamfilter. The filtered BAM files were then processed by metaDMG to obtain misincorporation matrices for each genome. The abundance tables, fragment length distribution, and misincorporation <sup>312</sup> matrices were then used in aMGSIM-smk v0.0.1 (Fernandez-Guerra, 2022b), a Snakemake workflow (Mölder et al., 2021) that facilitates the generation of multiple synthetic ancient metagenomes. The <sup>314</sup> underlying tools in this workflow is the gargamel toolkit (Renaud et al., 2017), that based on input read length distribution extract a subset of sequences (FragSim) with similar length. This is <sup>316</sup> then followed by the addition of  $C \rightarrow T$  substitutions (DeamSim) which mimics the postmortem damage process. Finally the deaminated sequences are passed to the ART (Huang et al., 2012) for <sup>318</sup> sequence simulation. The data used and generated by the workflow can be obtained from ERDA. We then performed taxonomic profiling and damage estimation using identical parameters as for <sup>320</sup> the synthetic reads generated by aMGSIM-smk.

## 4 | RESULTS

<sup>322</sup> We tested the accuracy and performance of the metaDMG damage estimates,  $D_{fit}$ , using a set of different simulation scenarios and subsequently tested on 9 real-life ancient metagenomic dataset.

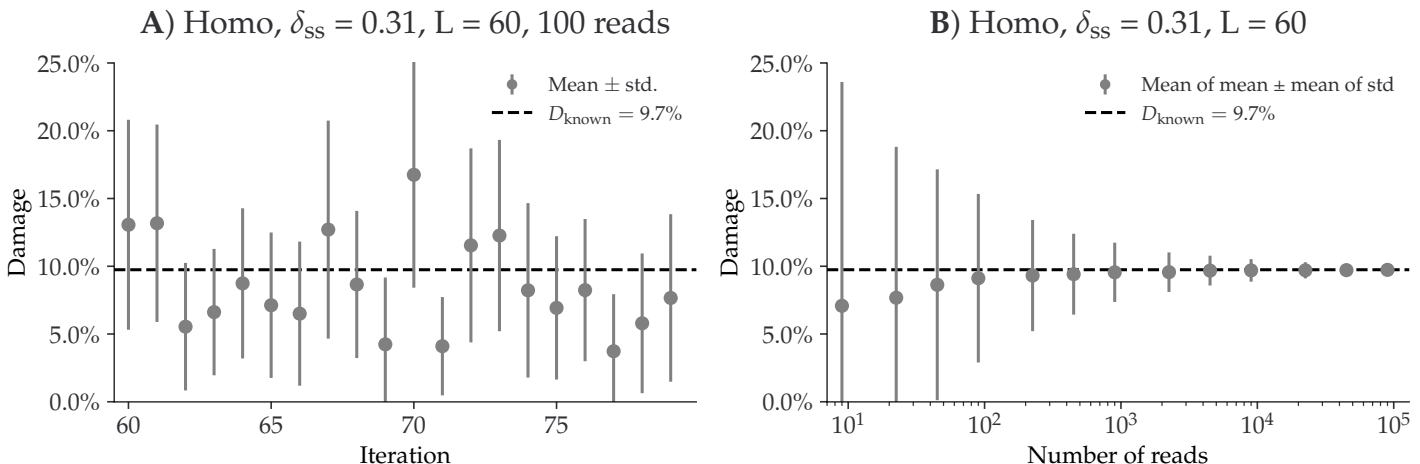


**Figure 3.** Overview of the single-genome simulations based on the Homo Sapiens genome with a fragment length distribution with mean 60 and the Briggs parameter  $\delta_{SS} = 0.31$  (approximately 10% damage). **A)** This plot shows the estimated damage ( $D_{fit}$ ) of 20 replicates, each with 100 reads. The grey points show the mean damage (with its standard deviation as errorbars). The known damage ( $D_{known}$ ) is shown as a dashed line, see eq. (9). **B)** This plot shows the average damage as a function of the number of reads. The grey points show the average of the individual means (with the average of the standard deviations as errors).

#### 324 4.1 | Single-genome simulation results

To illustrate the results the performance on single-genomes, we first focus on a single, specific set  
 326 of simulation parameters. This simulation is based on the Homo Sapiens genome with the Briggs  
 parameter  $\delta_{SS} = 0.31$  (approximately 10% damage) and a mean fragment length of 60. In general,  
 328 we use  $\delta = 0.0097$ ,  $\nu = 0.024$ , and  $\lambda = 0.36$  as Briggs parameters, while varying  $\delta_{SS}$  (Briggs et al.,  
 329 2007). We show the metaDMG damage results for the 100 independent replications in **Figure 3**. The  
 330 left part of the figure shows the individual metaDMG damage estimates for an arbitrary choice of 20  
 332 replications (iteration 60 to 79). When the damage estimates are very low, the distribution of  $D_{fit}$  is  
 skewed (restricted to positive values), sometimes leading to errorbars going into negative damage,  
 which represents unrealistic estimates. The right hand side of the figure visualizes the average  
 334 amount of damage based on all 100 replications across a varying number of reads. This shows  
 that the damage estimates converge to the known value with more data, and that one needs more  
 336 than 100 reads to even get strictly positive damage estimates (when including uncertainties) for  
 this specific set of simulation parameters.

338 Across multiple simulations, each with 8 different damage levels, 13 different numbers of reads,  
 and 100 replications, we find no significant difference in test statistic across different species (**Fig-**

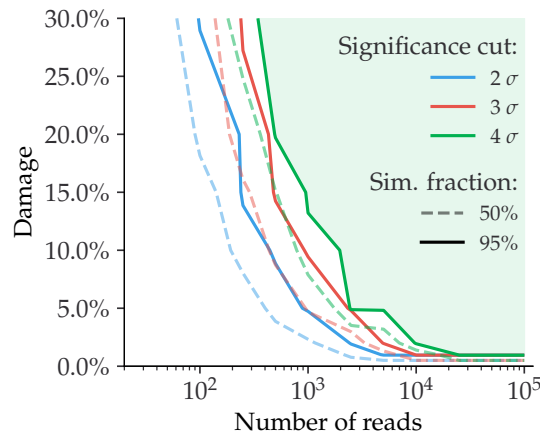


**Figure 4.** Relationship between the damage and the number of reads for simulated data (single-genome).

Given a specific significance cut, the solid contour line shows the relationship between the amount of damage and the number of reads required to be able to correctly infer damage in 95% of the taxa. The dashed line shows the similar value for a simulation fraction of 50%. The green part of the figure shows the “good” region of number of reads and estimated damage, given than one wants to be more than 95% certain of correctly identifying damage with more than  $4\sigma$  confidence.

ure S5 and Figure S6), across different GC-levels (Figure S7–Figure S9), different fragment length distributions (Figure S10–Figure S12), or even different contig lengths (Figure S13–Figure S15), see

342 **Appendix 4.** Based on the single-genome simulations, we compute the relationship between the  
amount of damage in a taxa and the number of reads required to correctly infer that the reads  
344 from that taxa are damaged, see **Figure 4**. If we want to assert damage with a significance of more  
than 2 (solid blue line) in a sample with around 5% expected damage, it requires about 1000 reads  
346 to be 95% certain that we will find results this good, whereas we only need 100 reads if our target  
organism has 30 % damage.

348 Finally, to quantify the risk of incorrectly classifying a non-ancient taxa as damaged, we created  
1000 independent replications for a varying number of reads, where none of them had any artificial  
350 ancient damage applied, only sequencing noise. **Figure 5** shows the damage ( $D_{\text{fit}}$ ) as a function of  
the significance ( $Z_{\text{fit}}$ ) for the case of 1000 reads. Even though the estimated damage is larger than  
352 zero, the damage is non-significant since the significance is less than one. When looking at all the  
figures across the different number of reads, see **Appendix 5**, we note that a relaxed significance  
354 threshold requiring that  $D_{\text{fit}} > 1\%$  and  $Z_{\text{fit}} > 2$  would filter out all of non-damaged points. Overall  
the conclusion being that our novel test statistic is conservative and has low false positive rate.

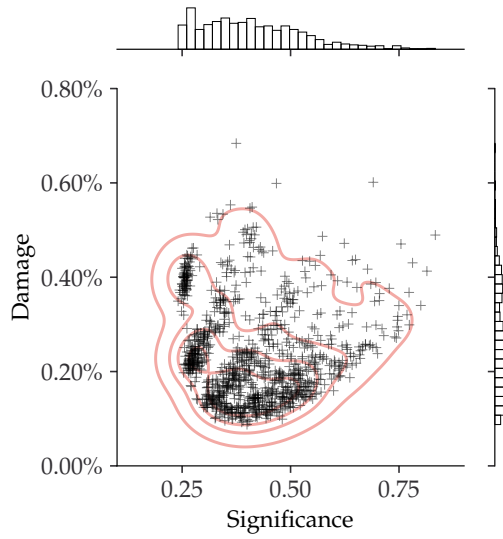


**Figure 5.** Inferred damage of modern, simulated data (single-genome). The plot shows the inferred damage estimates of 1000 replicates, each with 1000 reads and no artificial ancient damage applied. Each single cross corresponds to a simulation and the red lines outlines the kernel density estimate (KDE) of the damage estimates. The marginal distributions are shown as histograms next to the scatter plot.

## 356 4.2 | Metagenomic simulation results

With the full metagenomic simulation pipeline we can further probe the performance of `metaDMG`.

- 358 By considering the different metagenomic scenarios, see *Table 1*, at different steps in the pipeline, we are able to show that `metaDMG` provides relevant and accurate damage estimates.
- 360 To verify that the risk of getting false positives is non-significant, we run `metaDMG` on the metagenomic assemblages after fragmentation with `FragSim`, but before any deamination with `Deam-`
- 362 `Sim` has yet been added. We find that the previously established relaxed significance threshold ( $D_{\text{fit}} > 1\%$  and  $Z_{\text{fit}} > 2$ ) correctly filters out all of the taxa, see *Figure 6*. This is as expected, as there
- 364 has not yet been added any artificial post mortem damage in the form of deamination.

We see a clear difference in the damage estimates between the ancient and the non-ancient taxa once we add deamination with `DeamSim` and sequencing errors with `ART`, see *Figure 7*. The non-ancient taxa would still not pass the relaxed threshold, in contrast to the ancient samples.

- 368 The results of *Figure 7* are summarized in *Table 2*. We find that Cave-100-forward, Cave-102, Pitch-6 all have more than 60% of their ancient taxa correctly labelled as damaged according to the
- 370 relaxed threshold, while it for Cave-22 and Lake-7-forward is a bit lower. Lake-9 does not show any clear support of damage. However, once we condition on the requirement of having more than

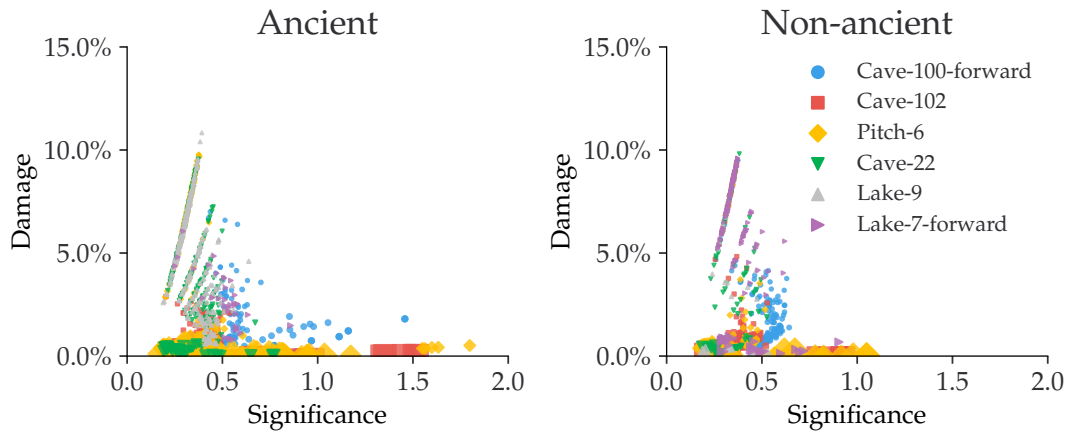


**Figure 6.** Estimated amount of damage as a function of significance for metagenomic simulations. This figure shows the metagenomic simulations after FragSim has been applied, but before including any deamination or sequencing errors. We generate both non-ancient and ancient taxa in the simulation pipeline. The left subfigure shows the damage of the ancient taxa and similarly for the non-ancient taxa in the right subfigure.

372 100 reads, the fraction of ancient taxa correctly identified as ancient increases to more than 90%  
 373 for most of the samples. A small investigation of one of the taxa that was simulated to be ancient  
 374 but misclassified by metaDMG, i.e. a false negative, can be found in [Appendix 6](#).

### 4.3 | Real Data

376 The results from running the full metaDMG pipeline on real data can be seen in [Figure 8](#). The figures  
 377 shows Blablabla, real life data here, XXX, Mikkel. We find that with the relaxed damage thresholds  
 378 ( $D_{\text{fit}} > 1\%$ ,  $Z_{\text{fit}} > 2$ ), metaDMG falsely classifies a single of the taxa from the control test Library-0  
 379 as being ancient. With a more conservative damage threshold ( $D_{\text{fit}} > 2\%$ ,  $Z_{\text{fit}} > 3$ , more than 100  
 380 reads), none of the taxa from the control test library would be classified as ancient.

### 4.4 | Bayesian vs. MAP

382 Due to the higher computational burden of computing the full Bayesian model compared to the  
 383 faster, approximate MAP model in samples with several thousand taxa, the MAP model is in prac-  
 384 tice the model of choice due to lower computational complexity. We compared the performance  
 385 of  $D_{\text{fit}}$  and  $Z_{\text{fit}}$  on the real datasets in [Table 1](#), see [Figure 9](#). This figure compares the estimated  
 386 damage between the Bayesian model and the MAP model (left subfigure) and the estimated sig-  
 387 nificances (right subfigure) for taxa passing a threshold of  $D_{\text{fit}} > 1\%$ ,  $Z_{\text{fit}} > 2$ , and more than 100  
 388 reads. The figure shows that the vast majority of taxa map 1:1 between the Bayesian and the MAP

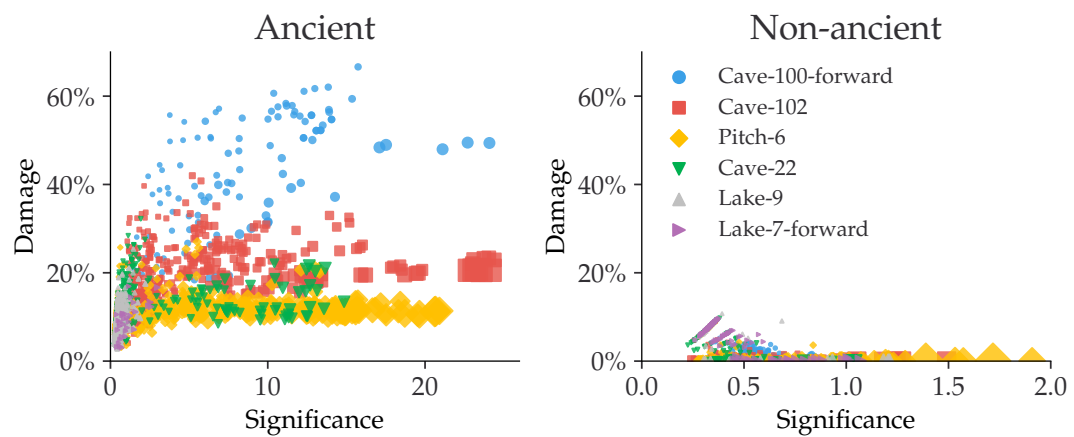


**Figure 7.** Estimated amount of damage as a function of significance for metagenomic simulations. This figure shows the metagenomic simulations after fragmentation, deamination, and sequencing errors have been applied. The left subfigure shows the damage of the ancient taxa and similarly for the non-ancient taxa in the right subfigure.

**Table 2.** metaDMG damage results for the six different metagenomic simulations. The first column is the total number of taxa, the second column is the total number of taxa that would pass the threshold of  $D_{fit} > 1\%$  and  $Z_{fit} > 2$ , the third column is the number of taxa with more than 100 reads, and the final column is the number of taxa with more than 100 reads that also do pass the cut.

| Sample           | Total | Pass | +100 Reads | +100 Reads and Pass |     |       |
|------------------|-------|------|------------|---------------------|-----|-------|
| Cave-100-forward | 135   | 107  | 79.3%      | 88                  | 87  | 98.9% |
| Cave-102         | 500   | 326  | 65.2%      | 309                 | 285 | 92.2% |
| Pitch-6          | 415   | 260  | 62.7%      | 274                 | 260 | 94.9% |
| Cave-22          | 393   | 71   | 18.1%      | 73                  | 69  | 94.5% |
| Lake-9           | 410   | 2    | 0.5%       | 8                   | 0   | 0%    |
| Lake-7-forward   | 32    | 4    | 12.5%      | 6                   | 4   | 66.7% |

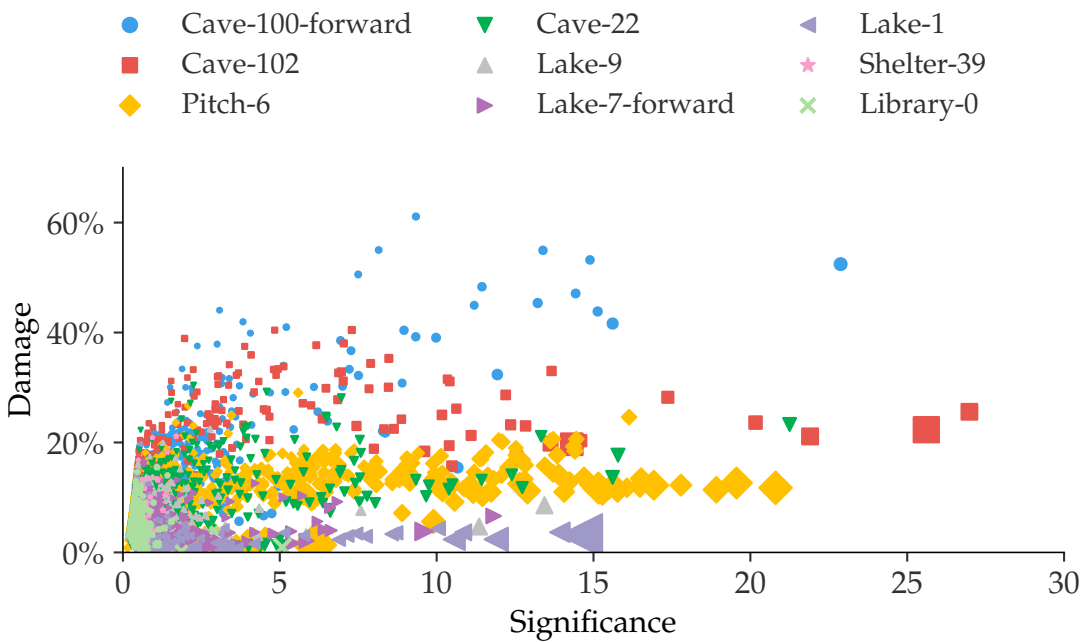


**Figure 8.** Estimated amount of damage as a function of significance using the real data, see [Table 1](#).

model. It should be noticed that the taxa with the worst correspondence in damage estimates  
 390 are all based on forward-only fits, i.e. with no information from the reverse strand, which leads  
 to less data to base the fits on. For the comparison with no thresholds applied, see [Figure S23](#) in  
 392 [Appendix 7](#). We recommend to use the full, Bayesian model in the case of extremely low-coverage  
 data or when used on only a small number of taxa (e.g. when using `metaDMG` in global-mode).

#### 394 4.5 | Existing Methods

To our knowledge there are not currently available methods for assessing and quantifying post-  
 396 mortem DNA damage in a metagenomic context. We compare the performance of the  $D_{fit}$  statistic  
 in `metaDMG` to existing methods such as those found in PyDamage (Borry et al., 2021). Since PyDam-  
 398 age is based solely on single genome analysis we use the non-LCA mode of `metaDMG`. This mode  
 iterates through the different referenceIDs for all mapped reads and estimates the damage for  
 400 each. In general, we find that `metaDMG` is more conservative, accurate and precise in its damage  
 estimates.

402 One example of this can be found in [Figure 10](#), which shows both the `metaDMG` and PyDamage  
 results of the simulations described in [subsection 3.1](#), in particular the 100 replications of the Homo  
 404 Sapiens single-genome with 100 reads and 15% added artificial damage (and a fragment length  
 distribution with mean 60). [Figure 10](#) shows that the `metaDMG` estimates are between 5% and 25%

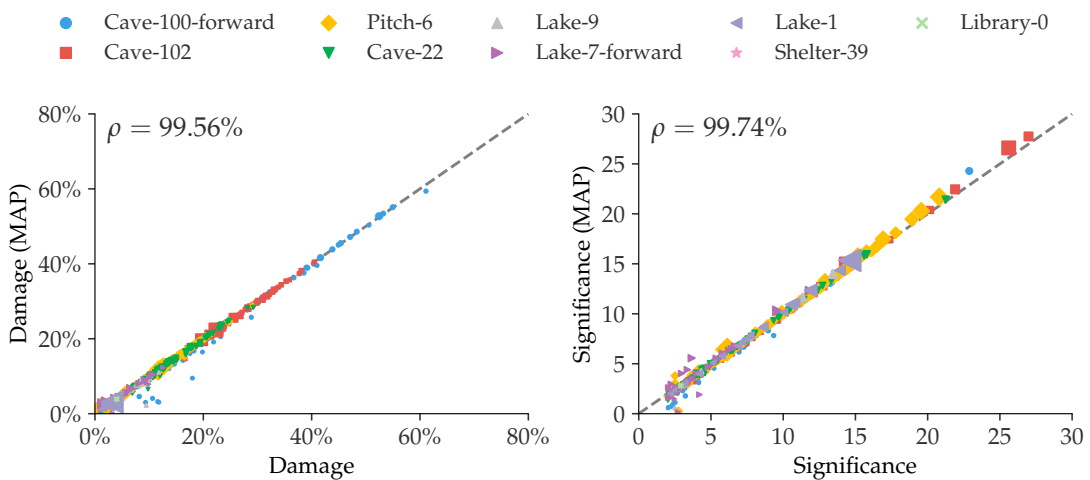


**Figure 9.** Comparison between the full Bayesian model and the fast, approximate, MAP model for the estimated damage and significance. The figure shows data after a loose cut of  $D_{\text{fit}} > 1\%$ ,  $Z_{\text{fit}} > 2$  and more than 100 reads. The dashed, grey line shows the 1:1 ratio and the correlation,  $\rho$ , is shown in the upper left corner.

406 damage, while PyDamage estimates up to more than 50% damage, in a sample with 15% artificially  
 407 added damage. The comparisons between metaDMG and PyDamage for the other sets of simulation  
 408 parameters can be found in *Figure S24–Figure S31* in *Appendix 8*.

To compare the computational performance, we use the real-life Pitch-6 sample (i.e. non-  
 410 simulated), see *Table 1*. This alignment file (in BAM-format) takes up 857 MB of space and has  
 411 3.7 millions reads with a total of 19 million alignments to 11.433 unique taxa. When using only  
 412 a single core, PyDamage took 1105s to compute all fits, while metaDMG took 88s, a factor of 12.6x  
 413 faster. The rest of the timings are shown in *Table 3*. PyDamage requires the alignment files to  
 414 be sorted by chromosome position and be supplied with an index file, allowing it to iterate fast  
 415 through the alignment file, at the expense of computational load before running the actual dam-  
 416 age estimation. metaDMG on the other hand requires the reads to be sorted by name to minimize  
 417 the time it takes to run the LCA.

## 418 5 | DISCUSSION

To our knowledge there are no currently available methods other than metaDMG that is geared to-  
 419 wards damage analysis in a metagenomic setting. It is the first general framework designed specif-  
 420 ically for the quantification of ancient damage in all contexts. The toolkit contains various inter-  
 421 linked and independent modules including a state-of-the-art graphical user interface that allow

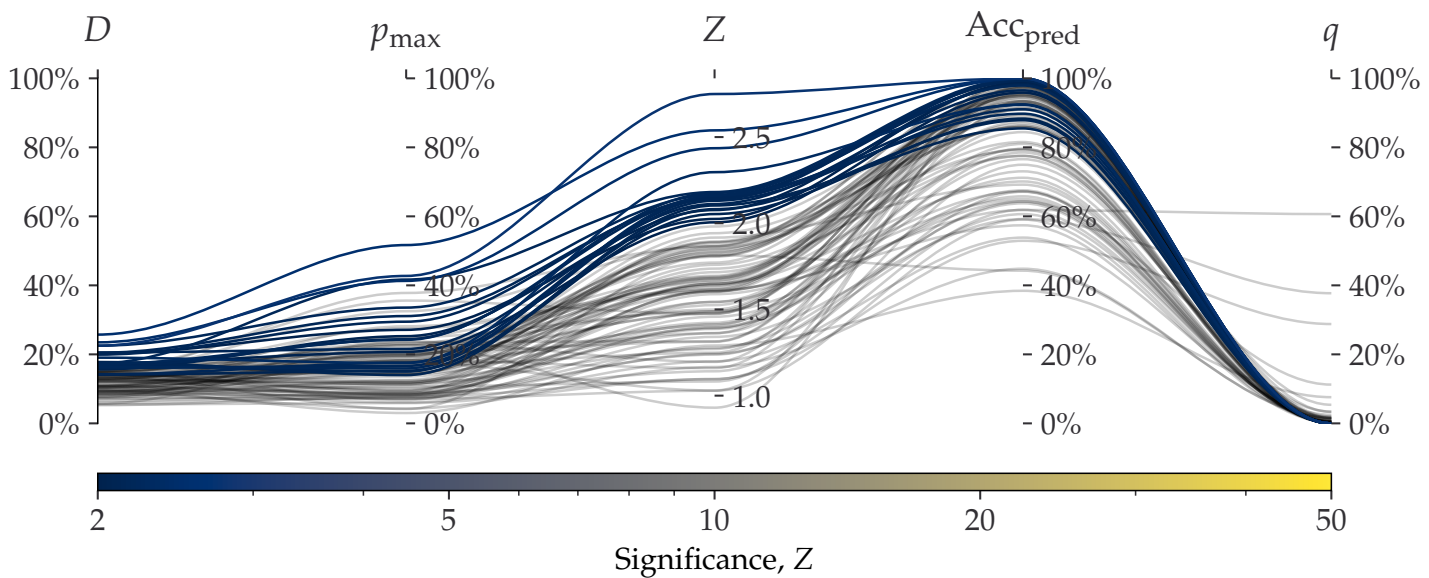


**Figure 10.** Parallel coordinates plot comparing `metaDMG` and `PyDamage` for the *Homo Sapiens* single-genome simulation with 100 reads and 15% added artificial damage. The two first axes show the estimated damage:  $D_{\text{fit}}$  by `metaDMG` and  $p_{\text{max}}$  by `PyDamage`. The following two axes show the fit quality: significance ( $Z_{\text{fit}}$ ) by `metaDMG` and the predicted accuracy ( $\text{Acc}_{\text{pred}}$ ) by `PyDamage`. The final axis shows the  $q$ -value by `PyDamage`. Each of the 100 replications are plotted as single lines. Replications passing the relaxed `metaDMG` damage threshold ( $D_{\text{fit}} > 1\%$  and  $Z_{\text{fit}} > 2$ ) are shown in color proportional to their significance. Replications that did not pass are shown in semi-transparent black lines.

**Table 3.** Computational performance of `PyDamage` and `metaDMG`. The table contains the times it takes to run either `PyDamage` or `metaDMG` on the full Pitch-6 sample containing 11,433 taxa. The timings are shown for both single-processing case (1 core) and multi-processing (2 and 4 cores). The timings were performed on a Macbook M1 Pro model from 2021. “12.6x” means that `metaDMG` was 12.6 times faster than `PyDamage` for that particular test.

| Cores | Pydamage (s) | metaDMG (s) | Improvement (x) |
|-------|--------------|-------------|-----------------|
| 1     | 1105         | 88 s        | 12.6            |
| 2     | 592          | 66 s        | 9.0             |
| 4     | 398          | 54 s        | 7.4             |

researchers to explore their data.

424        Multiple areas of future improvements exists. Currently, our novel test statistic for the damage  
425        estimation  $D_{\text{fit}}$  is based on a statistical model where we only consider the C→T and G→A transitions  
426        and where each taxa is modelled as being fully independent, even for closely related species when  
427        provided a taxonomic tree. This could be improved upon with the use of a hierarchical model  
428        were information across taxonomic leaf nodes is shared. The current implementation, however,  
429        allows for easy parallelization of the individual fits which reduces the time spent on the inference.  
430        In addition to the mismatch matrices, another improvement would be to include the read length  
431        distribution as a covariate in the damage model, as, in addition to deamination, the fragment length  
432        distribution is also an indicator of ancient damage (Dabney, Meyer, and Pääbo, 2013; Peyrégne and  
433        Prüfer, 2020).

434        We show that the  $D_{\text{fit}}$  statistic that metaDMG provides is accurate across different damage levels  
435        and different number of reads. In the single-genome reference case, we further show that the  
436        estimates are stable across different species and fragment length distributions. In addition to this,  
437        we find that the results are independent of the contig size, in contrast to PyDamage (Borry et al.,  
438        2021).

439        The basis for the  $D_{\text{fit}}$  statistic is the leaf node mismatch matrices which contains the raw ob-  
440        served substitution frequencies. The computation of these could also take into account the com-  
441        puted mapping uncertainty and the uncertainty of the assigned called nucleotide. We include a  
442        regression approach for stabilizing the mismatch matrices across all covariates but this requires  
443        much more data than our current approach. Rather than regressing on all covariates, it might also  
444        be more biological meaningfull to regress on the four Briggs parameters.

445        In our toolkit we have included the PMDtools approach (Skoglund et al., 2014) that allows for  
446        the separation of highly damaged reads from undamaged reads. The method offers a reasonable  
447        way to distinguish the endogenous ancient DNA from possible modern contamination. But this  
448        method may suffer from the fact that some fixed empirical parameters are applied. A possible  
449        extension can be using several statistics estimated from the specific sample (e.g., taxa specific  $D_{\text{fit}}$ ,  
450        and the ancient fragment lengths) as prior in an empirical Bayes inference framework to learn the  
451        categories of reads unsupervisedly.

452        Our research indicate that the metaDMG results are conservative with very low false positive rates.  
453        This is particularly important with metagenomic samples as the number of taxa, and thus the num-

454 ber of damage estimates, tend to be large. As the number of fits increases, we strongly believe that  
456 a graphical user interface is important to select and filter the fit results, and to better understand  
458 the data at hand. We have tested `metaDMG` using a state of the art metagenomic simulation pipeline  
based on multiple metagenomic real-life sample from a variety of different environments. In fu-  
ture studies, the simulation setup can further be improved by XXX (Mikkel, Antonio). We hope that  
460 `metaDMG` can improve the knowledge about DNA damage degradation in different environments  
and be the foundation of a more general, metagenomic ancient damage study.

## 6 | AUTHOR CONTRIBUTIONS

462 CM developed and implemented the damage model and all aspect of the python code including  
the CLI, all fits, and the dashboard. TP helped develop the model and with statistical discussions.  
464 TSK implemented the C/C++ code relating to the lowest common ancestor and mismatch matrices.  
LZ implemented the PMDtools and full multinomial regression subfunctionality. AFG and MWP  
466 designed the metagenomic simulation study and the application of `metaDMG` to real data. CM and  
MWP ran all analyses. CM, MWP and TSK initiated and designed the project. All authors contributed  
468 to writing the manuscript.

## REFERENCES

- 470 Ardelean, Ciprian F. et al. (2020). "Evidence of human occupation in Mexico around the Last Glacial Maximum". en. In: *Nature* 584.7819. Number: 7819 Publisher: Nature Publishing Group, pp. 87–92. ISSN: 1476-4687. DOI: [10.1038/s41586-020-2509-0](https://doi.org/10.1038/s41586-020-2509-0).
- 472 Betancourt, Michael (2018). "A Conceptual Introduction to Hamiltonian Monte Carlo". In: *arXiv:1701.02434* [stat]. arXiv: 1701.02434.
- 474 Borry, Maxime et al. (2021). "PyDamage: automated ancient damage identification and estimation for contigs in ancient DNA de novo assembly". en. In: *PeerJ* 9. Publisher: PeerJ Inc., e11845. ISSN: 2167-8359. DOI: [10.7717/peerj.11845](https://doi.org/10.7717/peerj.11845).
- 478 Braadbaart, F. et al. (2020). "Heating histories and taphonomy of ancient fireplaces: A multi-proxy case study from the Upper Palaeolithic sequence of Abri Pataud (Les Eyzies-de-Tayac, France)". en. In: *Journal of Archaeological Science: Reports* 33, p. 102468. ISSN: 2352-409X. DOI: [10.1016/j.jasrep.2020.102468](https://doi.org/10.1016/j.jasrep.2020.102468).
- 482 Bradbury, James et al. (2018). *JAX: composable transformations of Python NumPy programs*.
- 484 Briggs, Adrian W. et al. (2007). "Patterns of damage in genomic DNA sequences from a Neandertal". en. In: *Proceedings of the National Academy of Sciences* 104.37. Publisher: National Academy of Sciences Section: Biological Sciences, pp. 14616–14621. ISSN: 0027-8424, 1091-6490. DOI: [10.1073/pnas.0704665104](https://doi.org/10.1073/pnas.0704665104).
- 488 Cabanski, Christopher R. et al. (2012). "ReQON: a Bioconductor package for recalibrating quality scores from next-generation sequencing data". In: *BMC Bioinformatics* 13.1, p. 221. ISSN: 1471-2105. DOI: [10.1186/1471-2105-13-221](https://doi.org/10.1186/1471-2105-13-221).
- 490 Cepeda-Cuervo, Edilberto and MARÍA VICTORIA Cifuentes-Amado (2017). "Double Generalized Beta-Binomial and Negative Binomial Regression Models". en. In: *Revista Colombiana de Estadística* 40.1. Publisher: Universidad Nacional de Colombia., pp. 141–163. ISSN: 0120-1751. DOI: [10.15444/rce.v40n1.61779](https://doi.org/10.15444/rce.v40n1.61779).
- 494 Champlot, Sophie et al. (2010). "An efficient multistrategy DNA decontamination procedure of PCR reagents for hypersensitive PCR applications". eng. In: *PLoS One* 5.9, e13042. ISSN: 1932-6203. DOI: [10.1371/journal.pone.0013042](https://doi.org/10.1371/journal.pone.0013042).
- 498 Dabney, Jesse, Matthias Meyer, and Svante Pääbo (2013). "Ancient DNA Damage". In: *Cold Spring Harbor Perspectives in Biology* 5.7, a012567. ISSN: 1943-0264. DOI: [10.1101/cshperspect.a012567](https://doi.org/10.1101/cshperspect.a012567).

- Dembinski, Hans et al. (2021). *scikit-hep/iminuit*: v2.8.2. DOI: [10.5281/ZENODO.3949207](https://doi.org/10.5281/ZENODO.3949207).
- 500 Fellows Yates, James A. et al. (2021). "The evolution and changing ecology of the African hominid  
oral microbiome". en. In: *Proceedings of the National Academy of Sciences* 118.20, e2021655118.  
502 ISSN: 0027-8424, 1091-6490. DOI: [10.1073/pnas.2021655118](https://doi.org/10.1073/pnas.2021655118).
- Fernandez-Guerra, Antonio (2022a). *BAM-filter*. original-date: 2021-10-19T09:14:18Z.  
504 — (2022b). *genomewalker/aMGSIM-smk*: v0.0.1. DOI: [10.5281/zenodo.7298422](https://doi.org/10.5281/zenodo.7298422).
- Gilbert, M. Thomas P. et al. (2005). "Assessing ancient DNA studies". en. In: *Trends in Ecology &*  
506 *Evolution* 20.10, pp. 541–544. ISSN: 0169-5347. DOI: [10.1016/j.tree.2005.07.005](https://doi.org/10.1016/j.tree.2005.07.005).
- Ginolhac, Aurelien et al. (2011). "mapDamage: testing for damage patterns in ancient DNA se-  
508 quences". In: *Bioinformatics* 27.15, pp. 2153–2155. ISSN: 1367-4803. DOI: [10.1093/bioinformatics/btr347](https://doi.org/10.1093/bioinformatics/btr347).
- 510 Henriksen, Ramus, Lei Zhao, and Thorfinn Korneliussen (2022). *NGSNGS*: v0.5.0. DOI: [10.5281/zenodo.7326212](https://doi.org/10.5281/zenodo.7326212).
- 512 Huang, Weichun et al. (2012). "ART: a next-generation sequencing read simulator". eng. In: *Bioinfor-*  
*matics (Oxford, England)* 28.4, pp. 593–594. ISSN: 1367-4811. DOI: [10.1093/bioinformatics/btr708](https://doi.org/10.1093/bioinformatics/btr708).
- 514 Jensen, Theis Z. T. et al. (2019). "A 5700 year-old human genome and oral microbiome from chewed  
birch pitch". en. In: *Nature Communications* 10.1. Number: 1 Publisher: Nature Publishing Group,  
516 p. 5520. ISSN: 2041-1723. DOI: [10.1038/s41467-019-13549-9](https://doi.org/10.1038/s41467-019-13549-9).
- Jónsson, Hákon et al. (2013). "mapDamage2.0: fast approximate Bayesian estimates of ancient DNA  
518 damage parameters". en. In: *Bioinformatics* 29.13, pp. 1682–1684. ISSN: 1367-4803, 1460-2059.  
DOI: [10.1093/bioinformatics/btt193](https://doi.org/10.1093/bioinformatics/btt193).
- 520 Lam, Siu Kwan, Antoine Pitrou, and Stanley Seibert (2015). "Numba: a LLVM-based Python JIT com-  
piler". In: *Proceedings of the Second Workshop on the LLVM Compiler Infrastructure in HPC*. LLVM  
522 '15. New York, NY, USA: Association for Computing Machinery, pp. 1–6. ISBN: 978-1-4503-4005-2.  
DOI: [10.1145/2833157.2833162](https://doi.org/10.1145/2833157.2833162).
- 524 Langmead, Ben and Steven L. Salzberg (2012). "Fast gapped-read alignment with Bowtie 2". en. In:  
*Nature Methods* 9.4. Number: 4 Publisher: Nature Publishing Group, pp. 357–359. ISSN: 1548-  
526 7105. DOI: [10.1038/nmeth.1923](https://doi.org/10.1038/nmeth.1923).
- Llamas, Bastien et al. (2017). "From the field to the laboratory: Controlling DNA contamination in  
528 human ancient DNA research in the high-throughput sequencing era". en. In: *STAR: Science &*

530 2016.1258824.

McElreath, Richard (2020). *Statistical rethinking: a Bayesian course with examples in R and Stan*. 2nd ed.

532 CRC texts in statistical science. Boca Raton: Taylor and Francis, CRC Press. ISBN: 978-0-367-  
13991-9.

534 Mölder, Felix et al. (2021). *Sustainable data analysis with Snakemake*. en. Tech. rep. 10:33. Type: article. F1000Research. DOI: [10.12688/f1000research.29032.2](https://doi.org/10.12688/f1000research.29032.2).

536 Murchie, Tyler J. et al. (2021). "Collapse of the mammoth-steppe in central Yukon as revealed by ancient environmental DNA". en. In: *Nature Communications* 12.1. Number: 1 Publisher: Nature Publishing Group, p. 7120. ISSN: 2041-1723. DOI: [10.1038/s41467-021-27439-6](https://doi.org/10.1038/s41467-021-27439-6).

540 Nayfach, Stephen et al. (2021). "CheckV assesses the quality and completeness of metagenome-assembled viral genomes". en. In: *Nature Biotechnology* 39.5. Number: 5 Publisher: Nature Publishing Group, pp. 578–585. ISSN: 1546-1696. DOI: [10.1038/s41587-020-00774-7](https://doi.org/10.1038/s41587-020-00774-7).

542 NCBI Resource Coordinators (2018). "Database resources of the National Center for Biotechnology Information". In: *Nucleic Acids Research* 46.D1, pp. D8–D13. ISSN: 0305-1048. DOI: [10.1093/nar/gkx1095](https://doi.org/10.1093/nar/gkx1095).

546 Neukamm, Judith, Alexander Peltzer, and Kay Nieselt (2021). "DamageProfiler: fast damage pattern calculation for ancient DNA". In: *Bioinformatics* 37.20, pp. 3652–3653. ISSN: 1367-4803. DOI: [10.1093/bioinformatics/btab190](https://doi.org/10.1093/bioinformatics/btab190).

548 Parks, Donovan H. et al. (2018). "A standardized bacterial taxonomy based on genome phylogeny substantially revises the tree of life". en. In: *Nature Biotechnology* 36.10. Number: 10 Publisher: Nature Publishing Group, pp. 996–1004. ISSN: 1546-1696. DOI: [10.1038/nbt.4229](https://doi.org/10.1038/nbt.4229).

552 Pedersen, Mikkel et al. (2016). "Postglacial viability and colonization in North America's ice-free corridor". en. In: *Nature* 537.7618. Number: 7618 Publisher: Nature Publishing Group, pp. 45–49. ISSN: 1476-4687. DOI: [10.1038/nature19085](https://doi.org/10.1038/nature19085).

554 Peyrégne, Stéphane and Kay Prüfer (2020). "Present-Day DNA Contamination in Ancient DNA Datasets". en. In: *BioEssays* 42.9. \_eprint: <https://onlinelibrary.wiley.com/doi/pdf/10.1002/bies.202000081>, p. 2000081. ISSN: 1521-1878. DOI: [10.1002/bies.202000081](https://doi.org/10.1002/bies.202000081).

558 Phan, Du, Neeraj Pradhan, and Martin Jankowiak (2019). "Composable Effects for Flexible and Accelerated Probabilistic Programming in NumPyro". In: *arXiv:1912.11554 [cs, stat]*. arXiv: 1912.11554.

- Plotly, Technologies (2015). *Collaborative data science*. Place: Montreal, QC Publisher: Plotly Technologies Inc.
- Renaud, Gabriel et al. (2017). "gargammel: a sequence simulator for ancient DNA". eng. In: *Bioinformatics (Oxford, England)* 33.4, pp. 577–579. ISSN: 1367-4811. DOI: [10.1093/bioinformatics/btw670](https://doi.org/10.1093/bioinformatics/btw670).
- Schulte, Luise et al. (2021). "Hybridization capture of larch (*Larix Mill.*) chloroplast genomes from sedimentary ancient DNA reveals past changes of Siberian forest". en. In: *Molecular Ecology Resources* 21.3. \_eprint: <https://onlinelibrary.wiley.com/doi/pdf/10.1111/1755-0998.13311>, pp. 801–815. ISSN: 1755-0998. DOI: [10.1111/1755-0998.13311](https://doi.org/10.1111/1755-0998.13311).
- Skoglund, Pontus et al. (2014). "Separating endogenous ancient DNA from modern day contamination in a Siberian Neandertal". In: *Proceedings of the National Academy of Sciences* 111.6. Publisher: Proceedings of the National Academy of Sciences, pp. 2229–2234. DOI: [10.1073/pnas.1318934111](https://doi.org/10.1073/pnas.1318934111).
- Valk, Tom van der et al. (2021). "Million-year-old DNA sheds light on the genomic history of mammoths". en. In: *Nature* 591.7849. Number: 7849 Publisher: Nature Publishing Group, pp. 265–269. ISSN: 1476-4687. DOI: [10.1038/s41586-021-03224-9](https://doi.org/10.1038/s41586-021-03224-9).
- Vernot, Benjamin et al. (2021). "Unearthing Neanderthal population history using nuclear and mitochondrial DNA from cave sediments". In: *Science* 372.6542. Publisher: American Association for the Advancement of Science, eabf1667. DOI: [10.1126/science.abf1667](https://doi.org/10.1126/science.abf1667).
- Wang, Yucheng, Thorfinn Sand Korneliussen, et al. (2022). "ngsLCA—A toolkit for fast and flexible lowest common ancestor inference and taxonomic profiling of metagenomic data". In: *Methods in Ecology and Evolution* n/a.n/a. Publisher: John Wiley & Sons, Ltd. ISSN: 2041-210X. DOI: [10.1111/2041-210X.14006](https://doi.org/10.1111/2041-210X.14006).
- Wang, Yucheng, Mikkel Pedersen, et al. (2021). "Late Quaternary dynamics of Arctic biota from ancient environmental genomics". en. In: *Nature* 600.7887. Number: 7887 Publisher: Nature Publishing Group, pp. 86–92. ISSN: 1476-4687. DOI: [10.1038/s41586-021-04016-x](https://doi.org/10.1038/s41586-021-04016-x).
- Zavala, Elena I. et al. (2021). "Pleistocene sediment DNA reveals hominin and faunal turnovers at Denisova Cave". en. In: *Nature* 595.7867. Number: 7867 Publisher: Nature Publishing Group, pp. 399–403. ISSN: 1476-4687. DOI: [10.1038/s41586-021-03675-0](https://doi.org/10.1038/s41586-021-03675-0).

## Appendix 1

### PMDTOOLS

Three non-mutually exclusive events can lead to an observation of C→T or G→A (Skoglund et al., 2014), namely (i) a true biological polymorphism (occurring at rate  $\pi$ ), (ii) a sequencing errors (rate  $\epsilon$ , can be extracted from the base quality scores of the site on the sampled strand), and (iii) in the case of damaged DNA, the damaged nucleotide frequencies are assumed to be only related to its position from either termini of the ancient fragment (C→T from 5' end, and G→A from 3' end). The error probability of the postmortem nucleotide misincorporation is under the pmdtools model given by:

$$D_x = C + p(1 - p)^{|x|}, \quad (10)$$

here  $C = 0.01$  and  $p = 0.3$  are both suitable constants. Skoglund et al., 2014 defines the likelihood ratio of a strand between the PMD model and the NULL model as its postmortem damage score (PMDS),

$$\text{PMDS} = \log \left\{ \frac{\prod_x L(\text{PMD} | S_x)}{\prod_x L(\text{NULL} | S_x)} \right\}, \quad (11)$$

The reads with the PMDS exceeding an empirical p-value threshold can then be used for filtering intensively damaged fragments.

## Appendix 2

### MULTINOMIAL LOGISTIC REGRESSIONS

#### Full Multinomial Logistic Regression

Postmortem damages have impacts on the next generation sequencing reads. A common phenomenon is the increasing of the calling error rates from nucleotide C→T due to the cytosine deamination process. Unawareness of this will lead to inaccurate inferences. Evidences show that the magnitude of such changes are related to the positions the site is within a read (the fraction of the ancient DNA). Here we present four slightly different ways (i.e., full unconditional regression, full conditional regression, folded unconditional regression and folded conditional regression) to unveil the relationship between the calling error rates and the mismatching reference/read pairs as well as the site positions within a read. The methods are based on the multinomial logistic regressions.

#### Data Description

We perform the regressions based on the summary statistic of the mismatch matrix,i.e.,  $M(x)$ , which is a table which contains the counts of reads of different reference/read categories (in total 16) and positions on the forward/reversed strand (15 positions on each direction). *Table S1* and *Table S2* give an example of the data format we use for the inference.

| Ref. | Read Counts |      |       |       |       |         |       |         |
|------|-------------|------|-------|-------|-------|---------|-------|---------|
|      | A           |      |       |       | C     |         |       |         |
| Read | A           | C    | G     | T     | A     | C       | G     | T       |
| 1    | 12794053    | 8325 | 28769 | 16073 | 10404 | 8045811 | 8020  | 2092619 |
| 2    | 13480290    | 6812 | 21107 | 12102 | 9151  | 8260185 | 6531  | 1145605 |
| 3    | 12760253    | 6131 | 18859 | 10327 | 7772  | 8385423 | 5899  | 914709  |
| 4    | 12995572    | 5240 | 17671 | 8940  | 7880  | 8345892 | 5252  | 767237  |
| 5    | 12930102    | 4601 | 17021 | 8188  | 8374  | 8474964 | 5161  | 703283  |
| 6    | 12879355    | 4684 | 16435 | 7536  | 8726  | 8571141 | 4811  | 643607  |
| 7    | 12684349    | 4557 | 15298 | 7394  | 8835  | 8727254 | 4762  | 586674  |
| 8    | 12585563    | 4454 | 15497 | 7236  | 8898  | 8888173 | 5058  | 527691  |
| 9    | 12468622    | 4309 | 14704 | 6942  | 8948  | 9076851 | 4673  | 481170  |
| 10   | 12491183    | 4437 | 14567 | 6912  | 9103  | 9237982 | 4702  | 443329  |
| 11   | 12430899    | 4296 | 14083 | 6515  | 9313  | 9364121 | 4609  | 404431  |
| 12   | 12419506    | 4226 | 13985 | 6503  | 9342  | 9357468 | 4367  | 371475  |
| 13   | 12469412    | 4147 | 13851 | 6375  | 9586  | 9386737 | 4588  | 345390  |
| 14   | 12549936    | 4045 | 13650 | 6246  | 9673  | 9324488 | 4628  | 322294  |
| 15   | 12566555    | 4174 | 13499 | 6213  | 9735  | 9305820 | 4518  | 301360  |
| -1   | 11599167    | 8800 | 16164 | 14851 | 90888 | 9613102 | 10843 | 19810   |
| -2   | 11985637    | 8769 | 14044 | 12040 | 28799 | 9561124 | 7184  | 18424   |
| -3   | 12941743    | 7805 | 13861 | 12001 | 24988 | 9400151 | 6368  | 15466   |
| -4   | 12808985    | 7141 | 12885 | 9889  | 23067 | 9509723 | 5421  | 14901   |
| -5   | 12869585    | 6954 | 12100 | 9428  | 22349 | 9464831 | 5789  | 13987   |
| -6   | 12784911    | 6440 | 12080 | 8735  | 20556 | 9566794 | 6544  | 14021   |
| -7   | 12878349    | 5946 | 12311 | 8225  | 19480 | 9566359 | 6478  | 16419   |
| -8   | 12719722    | 9521 | 12156 | 8131  | 19226 | 9725468 | 6709  | 23434   |
| -9   | 12652860    | 5634 | 11940 | 7671  | 18035 | 9762224 | 6321  | 31667   |
| -10  | 12566817    | 5448 | 11850 | 7178  | 17353 | 9701382 | 6306  | 37831   |
| -11  | 12702498    | 5309 | 12092 | 7568  | 16121 | 9526031 | 6035  | 43215   |
| -12  | 12731940    | 5207 | 11933 | 6856  | 15637 | 9533858 | 5557  | 47650   |
| -13  | 12697647    | 4989 | 12199 | 7153  | 15072 | 9508117 | 5434  | 51614   |
| -14  | 12689924    | 4944 | 11891 | 6816  | 15050 | 9525285 | 5237  | 55598   |
| -15  | 12660634    | 4746 | 11753 | 6732  | 14815 | 9561359 | 5184  | 59633   |

626 **Appendix 2—table S1.** The read counts per position given the reference nucleotides are A or C of an  
 628 ancient human data. The negative position indices are the position on the reversed strand. In the  
 630 manuscript, the elements (the values of a specific nucleotide read counts per position given the  
 reference nucleotide is A or C) in this table are denoted as  $M_{A-i}(x)$  or  $M_{C-i}(x)$ .

| Ref. | Read Counts |      |         |       |       |       |      |          |
|------|-------------|------|---------|-------|-------|-------|------|----------|
|      | G           |      |         |       | T     |       |      |          |
| Read | A           | C    | G       | T     | A     | C     | G    | T        |
| 1    | 16389       | 8976 | 9639767 | 86584 | 11733 | 15878 | 8351 | 11718463 |
| 2    | 17614       | 6483 | 9510149 | 26655 | 10761 | 13958 | 7011 | 11974947 |
| 3    | 15164       | 5949 | 9488917 | 23374 | 9509  | 13767 | 6046 | 12839015 |
| 4    | 14844       | 5186 | 9566468 | 21960 | 8170  | 12509 | 5585 | 12721790 |
| 5    | 14005       | 5612 | 9497118 | 20468 | 7186  | 11991 | 5233 | 12795244 |
| 6    | 13671       | 6195 | 9622572 | 19096 | 6948  | 11683 | 4790 | 12686645 |
| 7    | 16648       | 6394 | 9609855 | 18594 | 6203  | 12122 | 4780 | 12794172 |
| 8    | 23659       | 6405 | 9768666 | 17341 | 6131  | 11847 | 4758 | 12626614 |
| 9    | 31680       | 6139 | 9785449 | 17034 | 5998  | 12040 | 4469 | 12579260 |
| 10   | 38484       | 5982 | 9700857 | 16235 | 5487  | 11546 | 4175 | 12513653 |
| 11   | 44665       | 5722 | 9536341 | 15284 | 5651  | 12044 | 4176 | 12646627 |
| 12   | 48949       | 5371 | 9547134 | 14569 | 5449  | 11663 | 4060 | 12684645 |
| 13   | 53076       | 5234 | 9543953 | 14090 | 5262  | 11785 | 4046 | 12631297 |
| 14   | 57343       | 5186 | 9551477 | 13855 | 5257  | 11768 | 4006 | 12624840 |
| 15   | 61236       | 5137 | 9583481 | 13667 | 5122  | 11733 | 3947 | 12612416 |
| -1   | 2078554     | 7947 | 8096447 | 11847 | 15732 | 28461 | 8551 | 12890628 |
| -2   | 1138478     | 6656 | 8232666 | 10760 | 12299 | 20759 | 6999 | 13446882 |
| -3   | 921712      | 5970 | 8399013 | 8643  | 10514 | 18226 | 6564 | 12718084 |
| -4   | 775038      | 5720 | 8319235 | 8416  | 9415  | 17800 | 5388 | 12977322 |
| -5   | 710955      | 5499 | 8462058 | 8926  | 8526  | 17088 | 4911 | 12886576 |
| -6   | 647761      | 5052 | 8545455 | 9193  | 7640  | 16351 | 4879 | 12852322 |
| -7   | 593854      | 4872 | 8693834 | 9318  | 7600  | 15523 | 5048 | 12664576 |
| -8   | 535542      | 7828 | 8889921 | 9399  | 7163  | 18704 | 4718 | 12510123 |
| -9   | 486549      | 4696 | 9075263 | 9522  | 7109  | 14547 | 4611 | 12409220 |
| -10  | 448895      | 4622 | 9226758 | 9432  | 6816  | 14567 | 4668 | 12438344 |
| -11  | 409027      | 4654 | 9352528 | 9544  | 6575  | 14019 | 4611 | 12388650 |
| -12  | 376069      | 4637 | 9344701 | 9419  | 6511  | 13874 | 4486 | 12390148 |
| -13  | 350609      | 4655 | 9384853 | 9885  | 6197  | 13877 | 4327 | 12432024 |
| -14  | 326760      | 4595 | 9337266 | 9889  | 5986  | 13928 | 4403 | 12490990 |
| -15  | 305014      | 4541 | 9310617 | 10065 | 5919  | 13442 | 4232 | 12529684 |

**Appendix 2—table S2.** The read counts per position given the reference nucleotides are G or T of the same human data as in Table S1. The negative position indices are the position on the reversed strand. In the manuscript, the elements (the values of a specific nucleotide read counts per position given the reference nucleotide is G or T) in this table are denoted as  $M_{G \rightarrow i}(x)$  or  $M_{T \rightarrow i}(x)$ .

The terminology used here might not be standard. The term full regression here is to distinguish itself from the folded regression discussed later, which simply means inferring the coefficients of forward strand and reversed strand separately. Full regression includes both unconditional regression and conditional regression. The unconditional regression's objective is to infer the probability of observing a read of nucleotide  $j$  and its reference is  $i$  at position  $x$ , i.e.,  $P_{i \rightarrow j}(x)$  while the conditional regression's target is to estimate the probability of observing a read of nucleotide  $j$  given its reference is  $i$  at position  $x$ , i.e.,  $P_{j|i}(x)$ . Their

relationship is as follows:

$$P_{j|i}(x) = \frac{P_{i \rightarrow j}(x)}{\sum_{j \in \mathcal{B}} P_{i \rightarrow j}(x)}.$$

So in fact, unconditional regression can give us more detailed inferred results (extra information the nucleotide composition per position of the reference, which may be related to the prepared libraries).

### Unconditional Regression Likelihood

The unconditional regression's log-likelihood function is defined as follows,

$$\begin{aligned} l_{\text{uncond}} &= \sum_x \sum_{i,j \in \mathcal{B}} M_{i \rightarrow j}(x) \log P_{i \rightarrow j}(x) \\ &= \sum_x \left[ M(x) \log P_{T \rightarrow T}(x) + \sum_{(i,j) \neq (T,T)} M_{i \rightarrow j}(x) \log \frac{P_{i \rightarrow j}(x)}{P_{T \rightarrow T}(x)} \right], \end{aligned} \quad (12)$$

where  $M(x) = \sum_{i,j \in \mathcal{B}} M_{i \rightarrow j}(x)$ . According to the multinomial logistic regression, we assume,

$$\log \frac{P_{i \rightarrow j}(x)}{P_{T \rightarrow T}(x)} = \sum_{n=0}^{\text{order}} \alpha_{i,j,x,n} x^n \quad (13)$$

Applying Equation 13 to Equation 12, we have

$$l_{\text{uncond}} = \sum_x \left\{ -M(x) \log \left[ 1 + \sum_{(i,j) \neq (T,T)} \exp \left( \sum_{n=0}^{\text{order}} \alpha_{i,j,x,n} x^n \right) \right] + \sum_{(i,j) \neq (T,T)} M_{i \rightarrow j}(x) \sum_{n=0}^{\text{order}} \alpha_{i,j,x,n} x^n \right\} \quad (14)$$

The number of inferred parameters ( $\alpha_{i,j,x,n}$ ), for the full conditional regression is  $30 \times (\text{order} + 1)$ .

And the relevant derivatives of the unconditional regression likelihood are as follows,

$$\frac{\partial l_{\text{uncond}}}{\partial \alpha_{i,j,x,n}} = -M(x) \frac{x^n \exp \left( \sum_{n=0}^{\text{order}} \alpha_{i,j,x,n} x^n \right)}{1 + \sum_{(i,j) \neq (T,T)} \exp \left( \sum_{n=0}^{\text{order}} \alpha_{i,j,x,n} x^n \right)} + M_{i \rightarrow j}(x) x^n. \quad (15)$$

### Conditional Regression Likelihood

Viewed as the sum of log-likelihoods given the reference nucleotide  $i \in \mathcal{B}$ , the conditional regression's log-likelihood function is,

$$\begin{aligned} l_{\text{cond}} &= \sum_{i \in \mathcal{B}} \sum_x \sum_{j \in \mathcal{B}} M_{i \rightarrow j}(x) \log P_{j|i}(x) \\ &= \sum_{i \in \mathcal{B}} \sum_x \left[ M_i(x) \log P_{T|i}(x) + \sum_{j \neq T} M_{i \rightarrow j}(x) \log \frac{P_{j|i}(x)}{P_{T|i}(x)} \right], \end{aligned} \quad (16)$$

where  $M_i(x) = \sum_{j \in B} M_{i \rightarrow j}(x)$ . Furthermore, if we assume,

$$\log \frac{P_{j|i}(x)}{P_{T|i}(x)} = \sum_{n=0}^{\text{order}} \beta_{i,j,x,n} x^n \quad (17)$$

By applying Equation 17 to Equation 16, we can obtain,

$$l_{\text{cond}} = \sum_{i \in B} \sum_x \left\{ -M_i(x) \log \left[ 1 + \sum_{j \neq T} \exp \left( \sum_{n=0}^{\text{order}} \beta_{i,j,x,n} x^n \right) \right] + \sum_{j \neq T} M_{i \rightarrow j}(x) \sum_{n=0}^{\text{order}} \beta_{i,j,x,n} x^n \right\} \quad (18)$$

The number of inferred parameters ( $\beta_{i,j,x,n}$ ) for the full unconditional regression is  $24 \times (\text{order} + 1)$ . And the relevant derivatives of the conditional likelihood are as follows,

$$\frac{\partial l_{\text{cond}}}{\partial \beta_{i,j,x,n}} = -M_i(x) \frac{x^n \exp \left( \sum_{n=0}^{\text{order}} \beta_{i,j,x,n} x^n \right)}{1 + \sum_{j \neq T} \exp \left( \sum_{n=0}^{\text{order}} \beta_{i,j,x,n} x^n \right)} + M_{i \rightarrow j}(x) x^n. \quad (19)$$

### Folded Multinomial Logistic Regression

The folded regressions use the same log-likelihood functions as the full regression (i.e., Equation 14 and 18) but are conducted based on a presumable symmetric PMD pattern, i.e., the probability of  $C \rightarrow T$  at the position  $x$  of an random chosen ancient DNA strand is assumed to equal to the probability of  $G \rightarrow A$  at the position  $-x$ . Such an theoretical assumption go match the current ancient library preparation process (Dabney, Meyer, and Pääbo, 2013; Henriksen, Zhao, and T. Korneliussen, 2022).

$$\alpha_{i,j,x,n} = \alpha_{c(i),c(j),-x,n}, \quad (20)$$

$$\beta_{i,j,x,n} = \beta_{c(i),c(j),-x,n}, \quad (21)$$

where  $c(i)$  means the complimentary nucleotide of the nucleotide  $i$ , e.g.,  $c(A) = T$  and  $c(G) = C$ .

By doing the folded regression, we halve the number of inferred parameters ( $\alpha_{i,j,x,n}$  or  $\beta_{i,j,x,n}$ ). Hence The number of inferred parameters for the folded unconditional regression is  $15 \times (\text{order} + 1)$ , and that of folded conditional regression is  $12 \times (\text{order} + 1)$ .

### Results for multinomial logistic regression

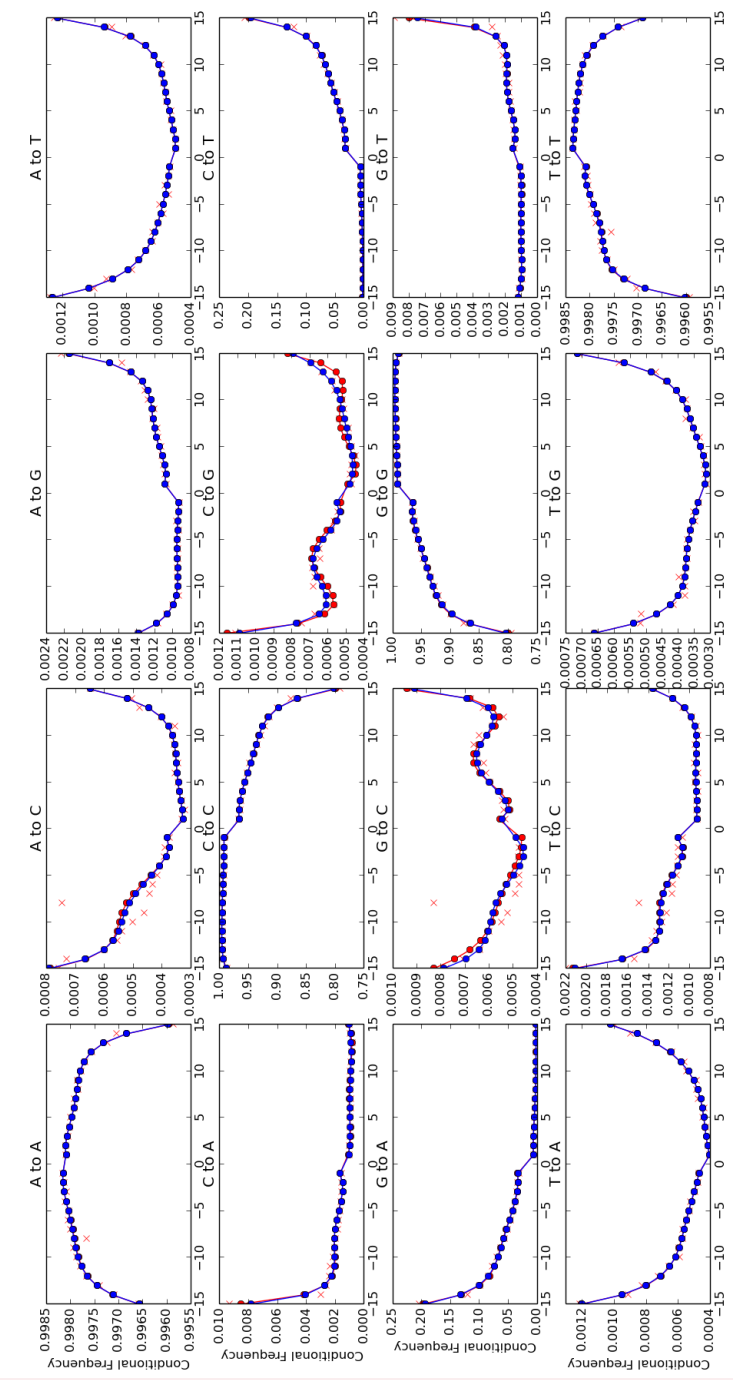
The optimization of the likelihood functions are based on the C++ library of gsl and use the function `gsl_multimin_fminimizer_nmsimplex2` with the initial searching point set to be the results of logistic regression. We here present here 4 figures pertaining to showcase the

performance of our model. The regression methods are based on the summary statistic of the counts of mismatches and the optimization is therefore in the scale of milliseconds.

*Figure S1* and *Figure S2* are the conditional regression results of the ancient and control human data correspondingly. And *Figure S3* and *Figure S4* are the folded conditional regression results of the same data as above.

712

Conditional Regression: order = 4, log-likelihood is -34526.568889, AIC is 69173.137778, BIC is 70313.881805

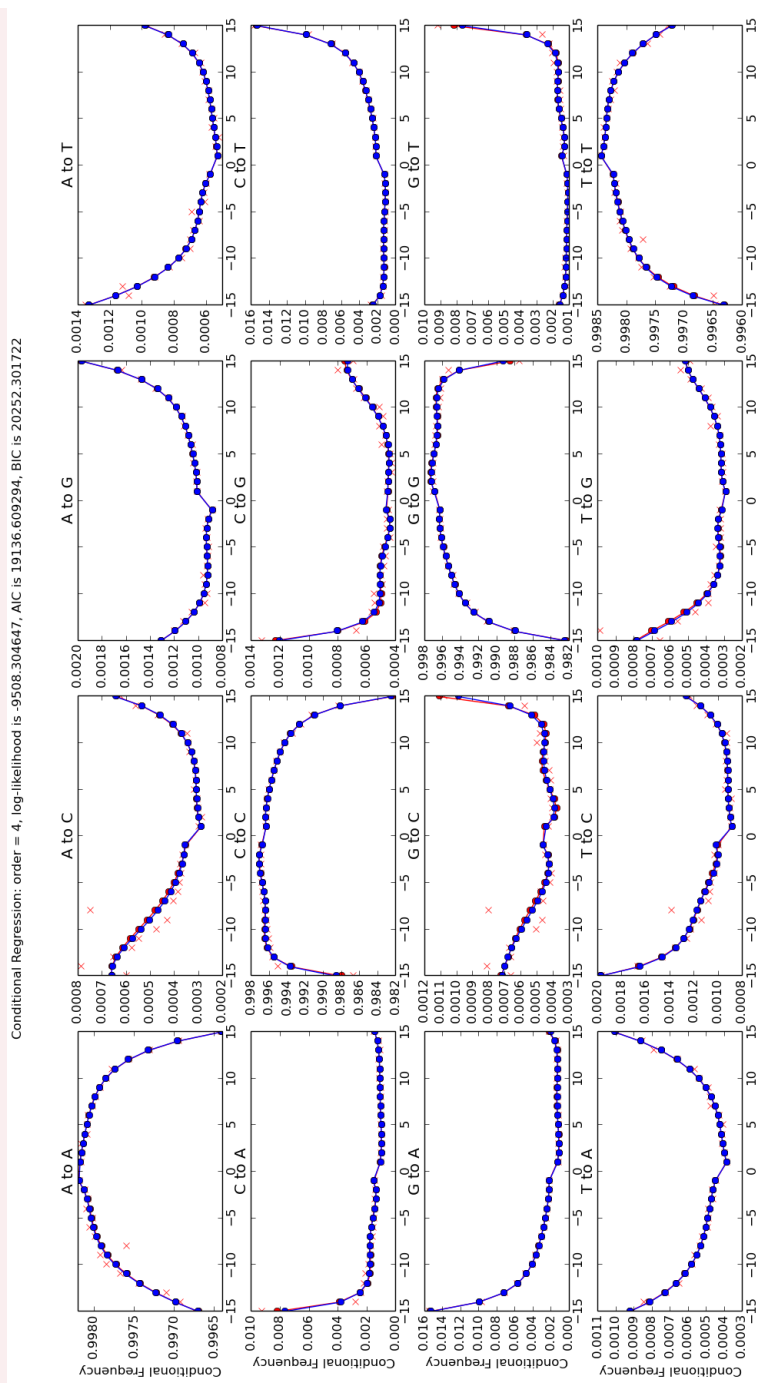


714

**Appendix 2—figure S1.** Conditional regression results with the order 4 of the ancient human data.

Each panel of figure represents a specific reference/read pair and plots its frequency across different positions. The positions from left to right are  $-1$  to  $-15$  and  $1$  to  $15$ .

716



718

#### Appendix 2—figure S2. Conditional regression results with the order 4 of the control human data.

720

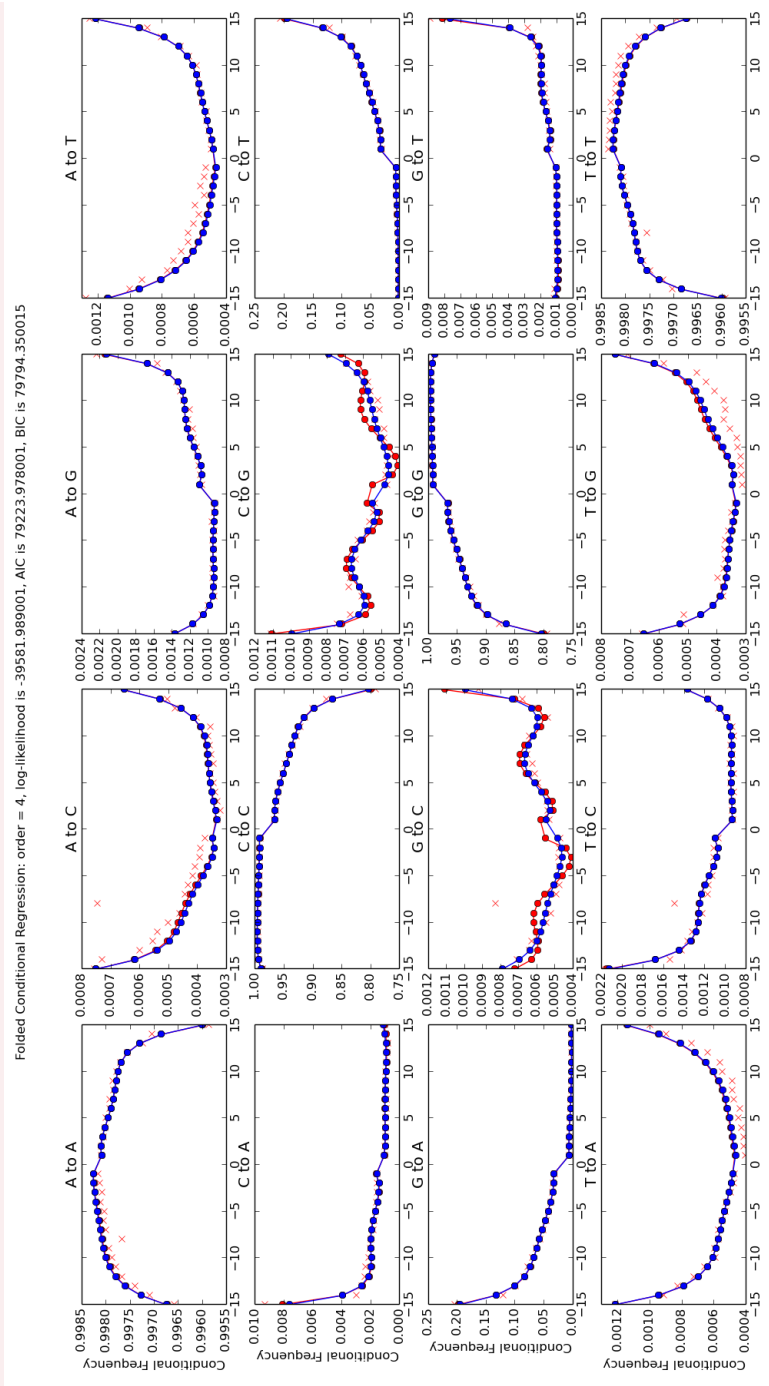
Each panel of figure represents a specific reference/read pair and plots its frequency across different positions. The positions from left to right are  $-1$  to  $-15$  and  $1$  to  $15$ .

722

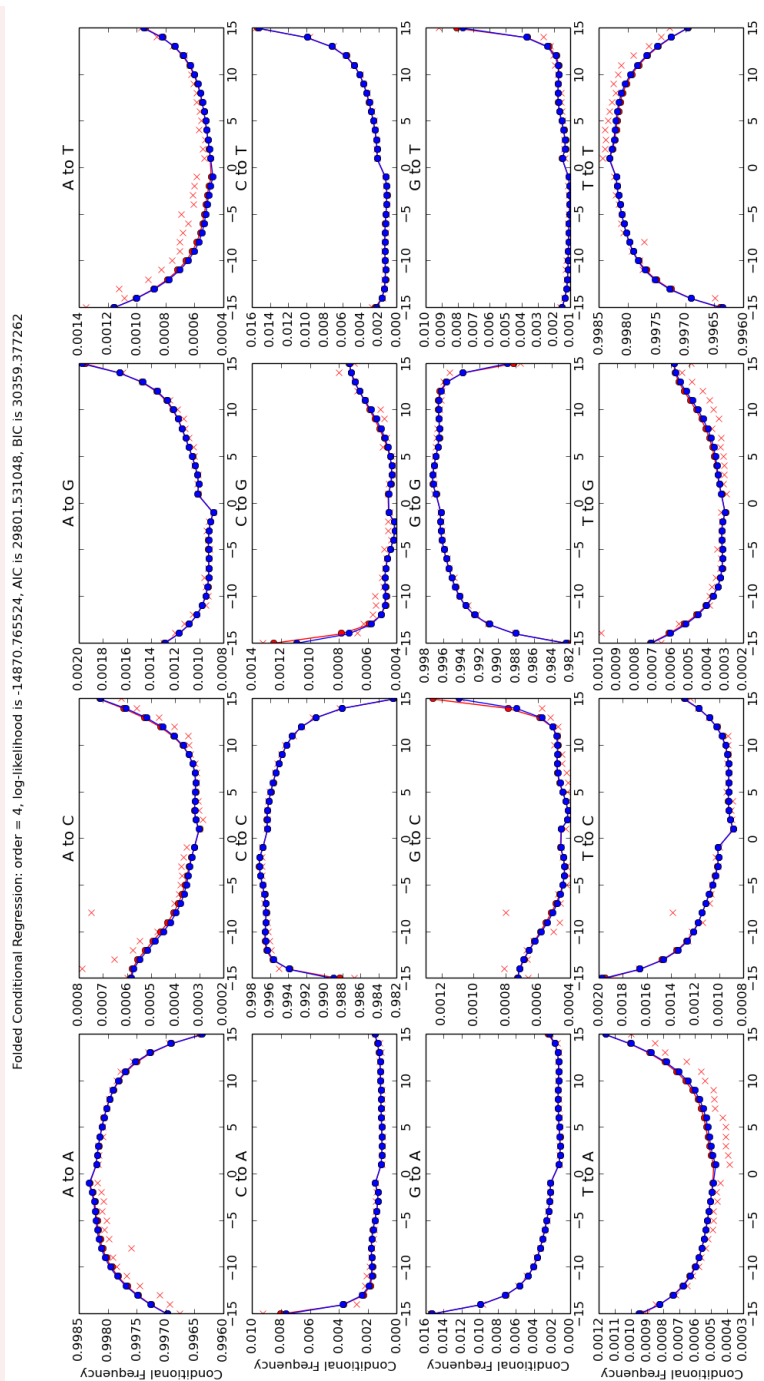
724

726

Folded Conditional Regression, order = 4, log-likelihood is -39581.989001, AIC is 79223.978001, BIC is 79794.350015



**Appendix 2—figure S3.** Folded conditional regression results with the order 4 of the ancient human data. Each panel of figure represents a specific reference/read pair and plots its frequency across different positions. The positions from left to right are  $-1$  to  $-15$  and  $15$  to  $1$ .



728

**Appendix 2—figure S4.** Folded conditional regression results with the order 4 of the control human data. Each panel of figure represents a specific reference/read pair and plots its frequency across different positions. The positions from left to right are  $-1$  to  $-15$  and  $1$  to  $15$ .

730

732 As shown in the figures, the regression models stabilize the coarse mismatch matrices  
734 and describe a much more detailed PMD pattern (not only C→T and G→A, but also all other  
736 reference and read combinations), but they might suffer from an overfitting issue espe-  
738 cially when the data is limited, while the simpler regression model in the main text (*sub-*  
*section 2.4*) shows an acceptable statistic power even with extremely small amount of data,  
we thus recommend the readers to use the simpler regression model unless used with ex-  
tremely high-coverage data.

740 Our code can also perform the unconditional regression, but as the unconditional regres-  
sion needs to estimate more parameters based on the same dataset, it is more vulnerable  
to a possible overfitting issue. We thus only present the figures of the conditional results.

## NGSNGS COMMANDS

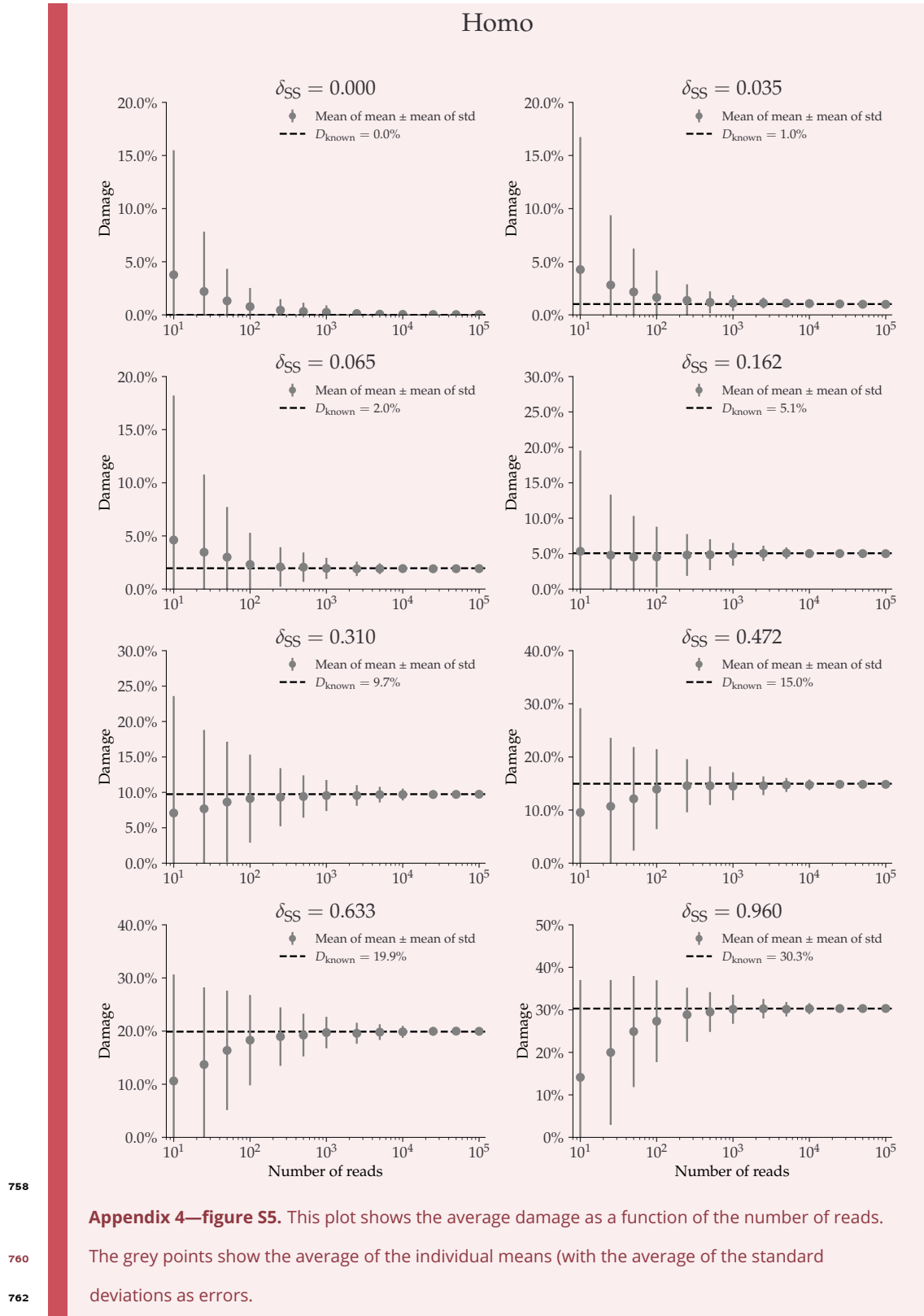
744 The resulting read data files (fastq files) were simulated with NGSNGS using the above  
745 mentioned simulation parameters, all with the same quality scores profiles as used in ART  
746 (Huang et al., 2012), based on the Illumina HiSeq 2500 (150 bp). The mapping was performed  
using Bowtie-2 (Langmead and Salzberg, 2012):

748     ./ngsngs -i \$genome -r \$Nread -ld LogNorm,\$lognorm\_mean,\$lognorm\_std -seq SE \  
749         -f fq -q1 \$quality\_scores -m b,0.024,0.36,\$damage,0.0097 -o \$fastq  
750         bowtie2 -x \$genome -q \$fastq.fq --no-unal

## Appendix 4

### 752 NGSNGS SIMULATIONS

754 The following figures show the metaDMG damage estimates for the different NGSNGS simu-  
756 lations (Henriksen, Zhao, and T. Korneliussen, 2022). These simulations include different  
species (*Homo Sapiens* and *Betula*), different GC-levels (low, middle, high), different frag-  
ment length distributions (with mean 35, 60, and 90), and different contig lengths (length  
1.000, 10.000, 100.000), see **subsection 3.1** for more information.

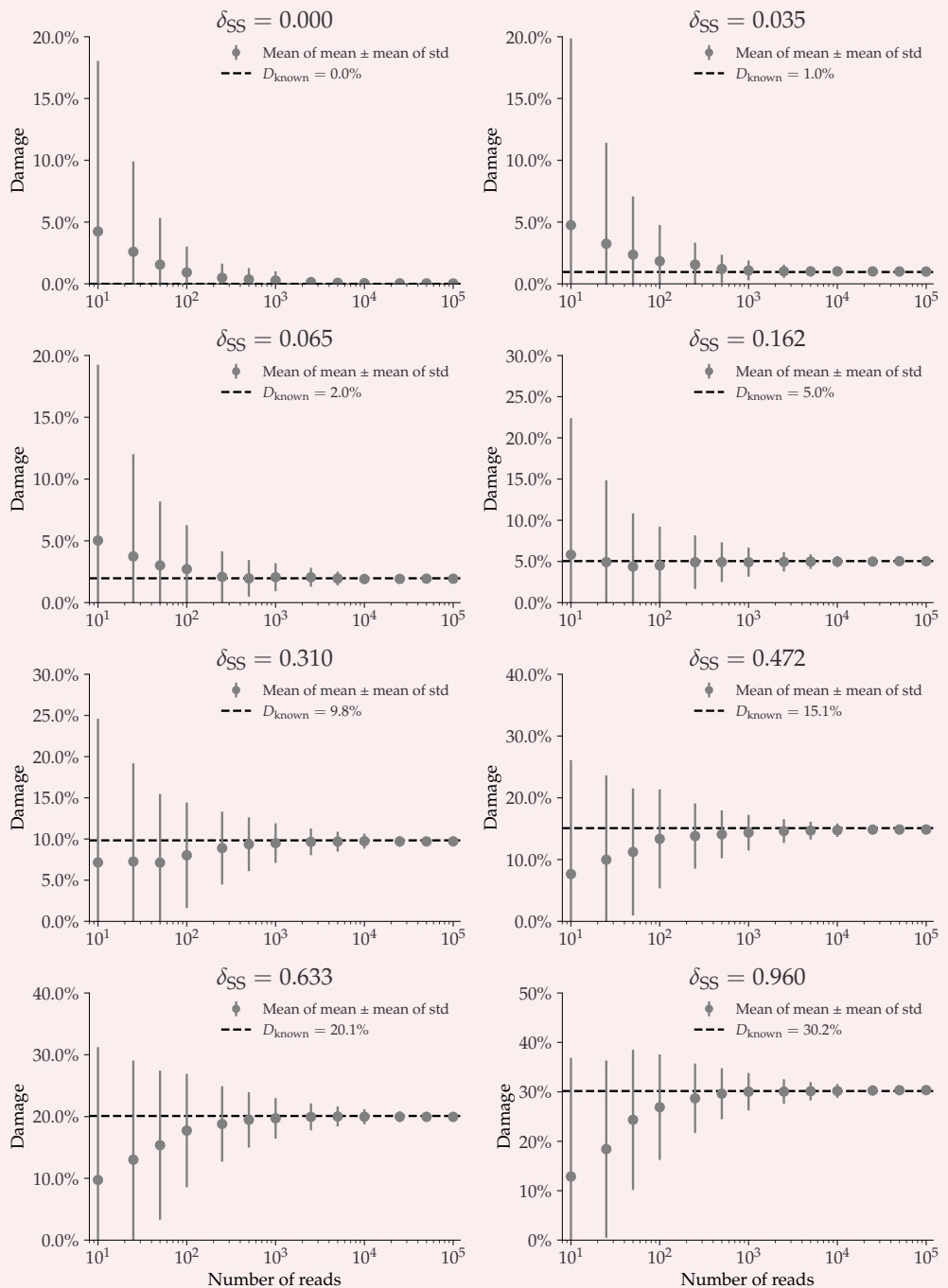


758

760

762

## Betula

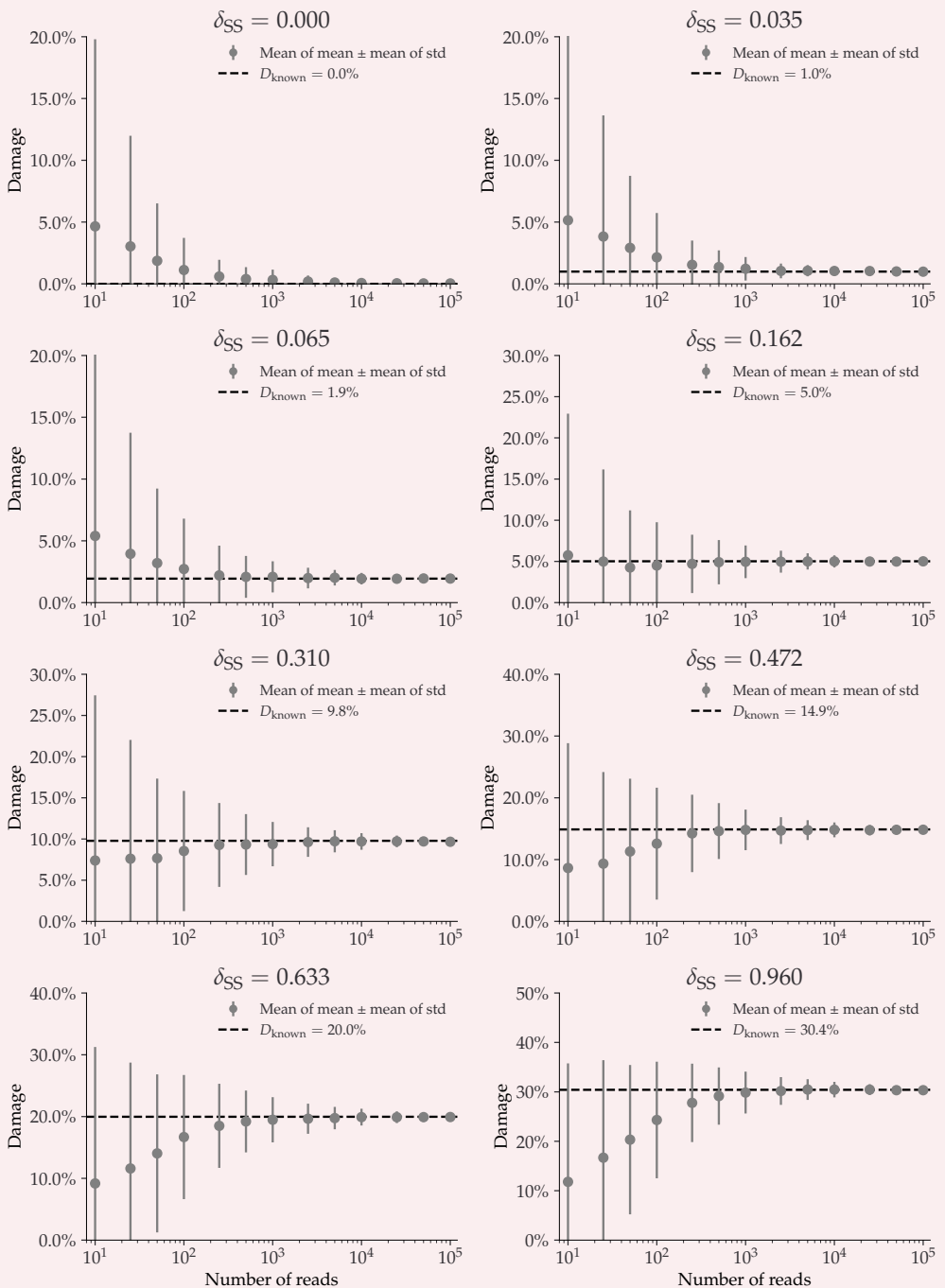


764

**Appendix 4—figure S6.** This plot shows the average damage as a function of the number of reads. The grey points show the average of the individual means (with the average of the standard deviations as errors).

766

## GC-low



768

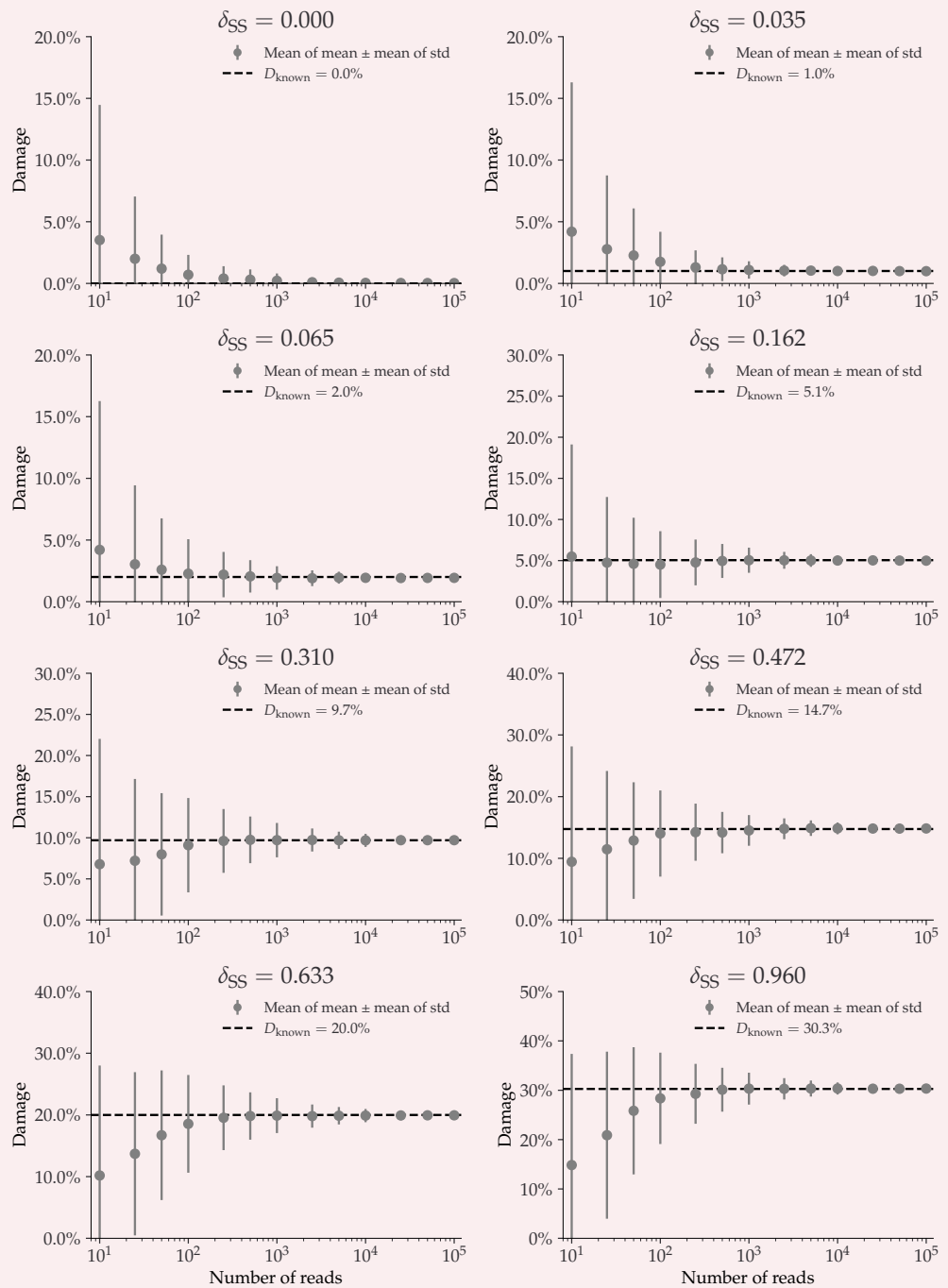
**Appendix 4—figure S7.** This plot shows the average damage as a function of the number of reads.

770

The grey points show the average of the individual means (with the average of the standard deviations as errors).

772

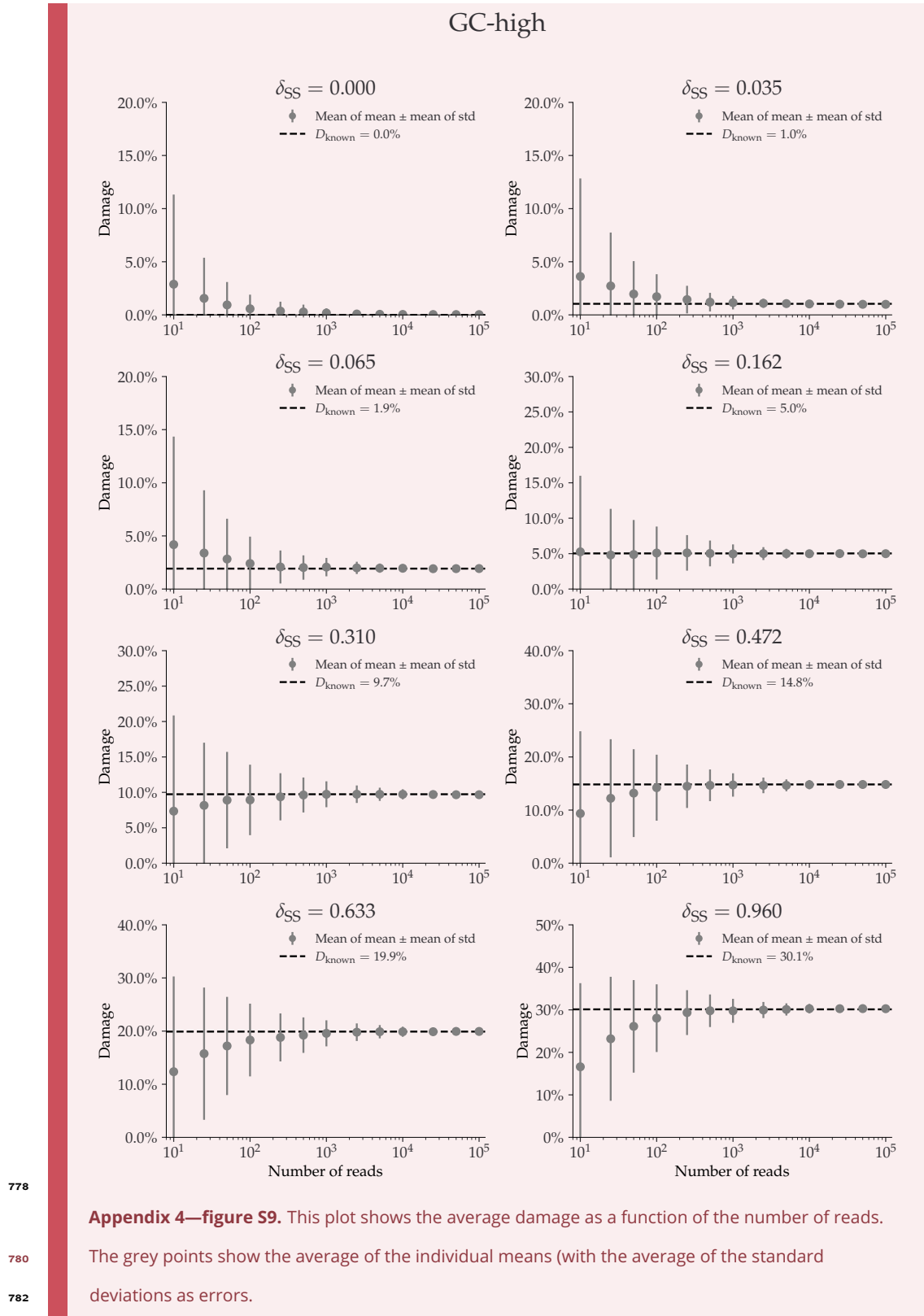
## GC-mid



774

**Appendix 4—figure S8.** This plot shows the average damage as a function of the number of reads. The grey points show the average of the individual means (with the average of the standard deviations as errors).

776



778

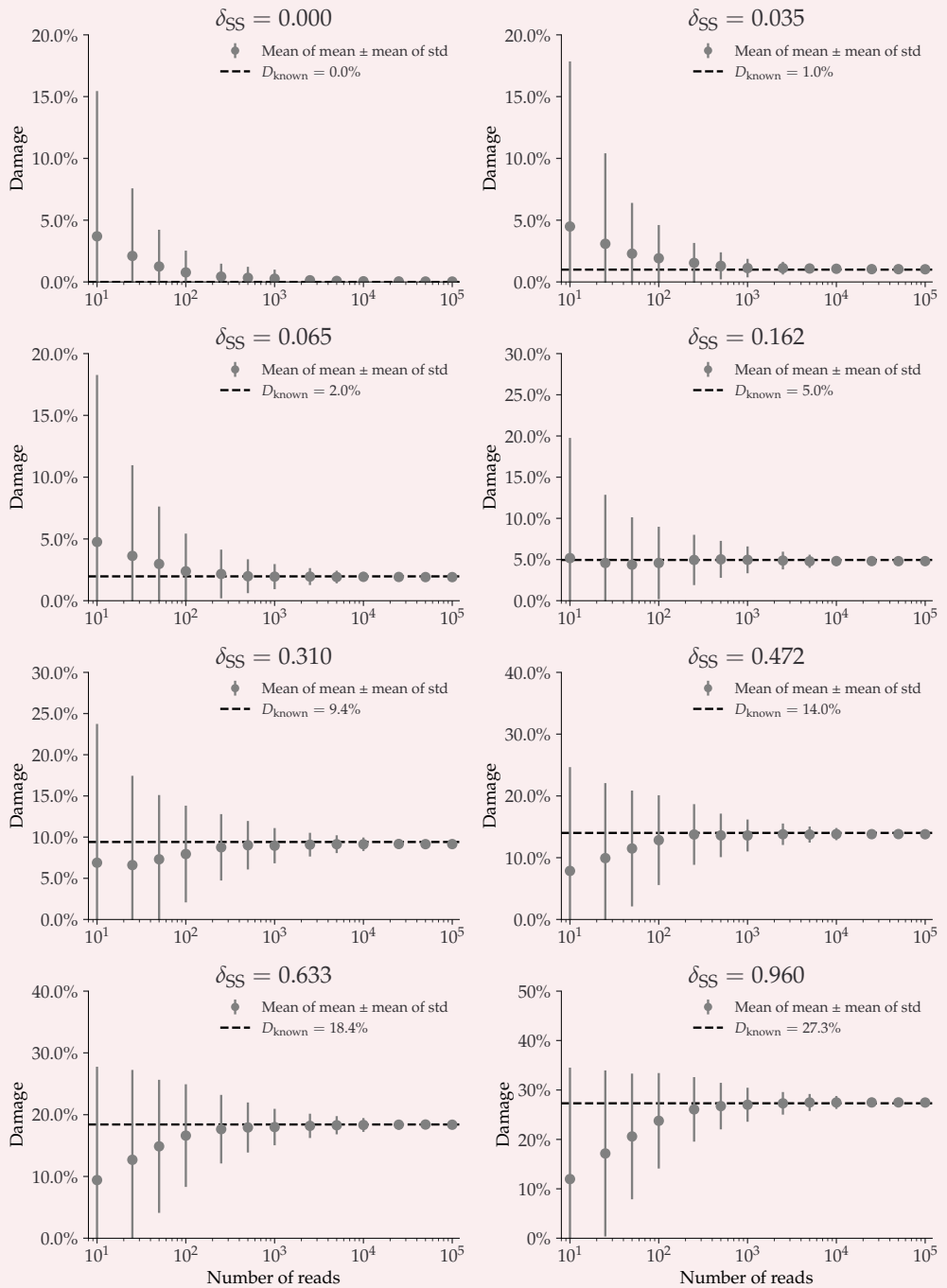
**Appendix 4—figure S9.** This plot shows the average damage as a function of the number of reads.

780

The grey points show the average of the individual means (with the average of the standard deviations as errors).

782

## Fragment Length Average: 35



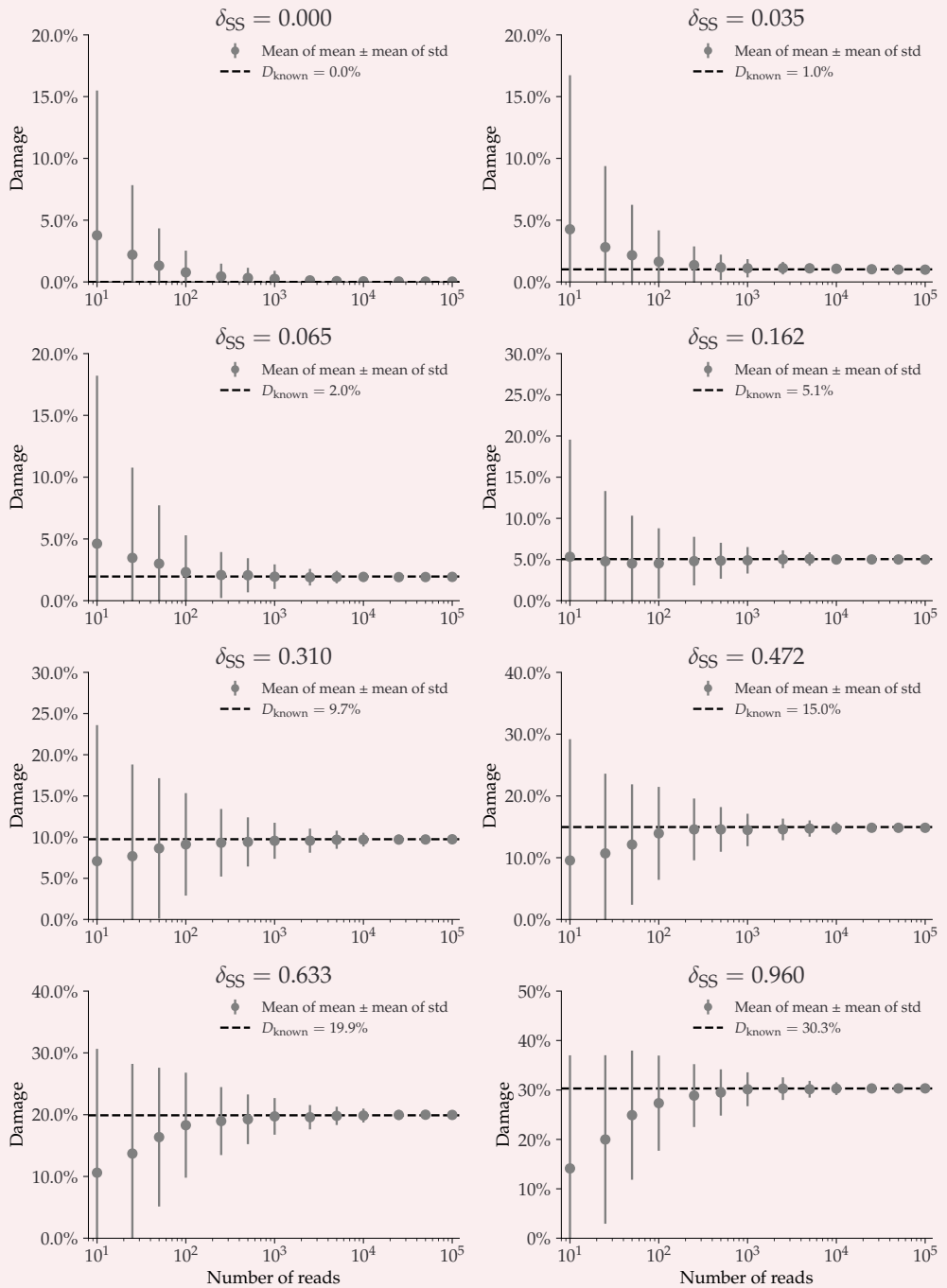
784

**Appendix 4—figure S10.** This plot shows the average damage as a function of the number of reads.

786

The grey points show the average of the individual means (with the average of the standard deviations as errors).

## Fragment Length Average: 60



788

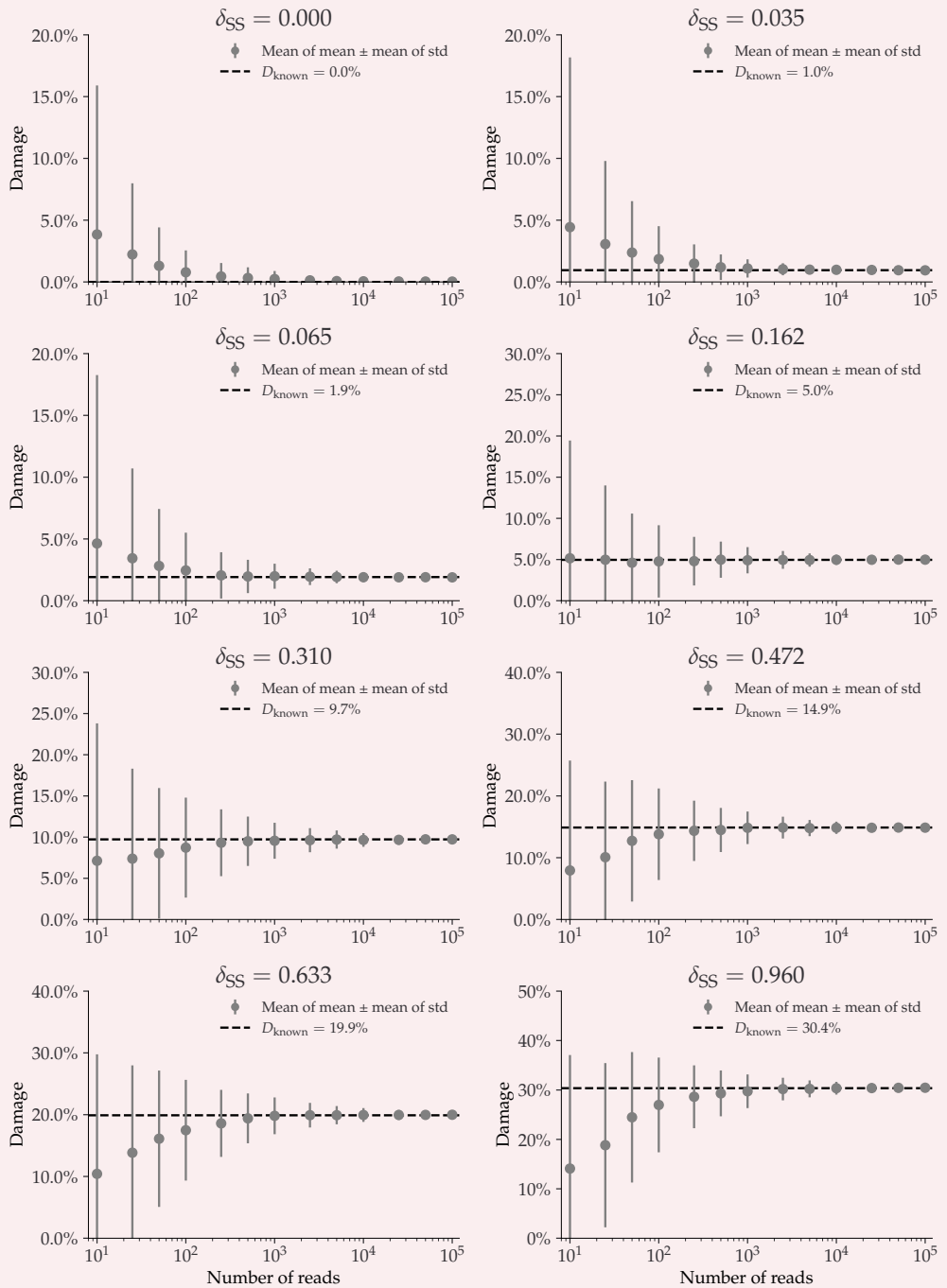
**Appendix 4—figure S11.** This plot shows the average damage as a function of the number of reads.

790

The grey points show the average of the individual means (with the average of the standard deviations as errors).

792

## Fragment Length Average: 90



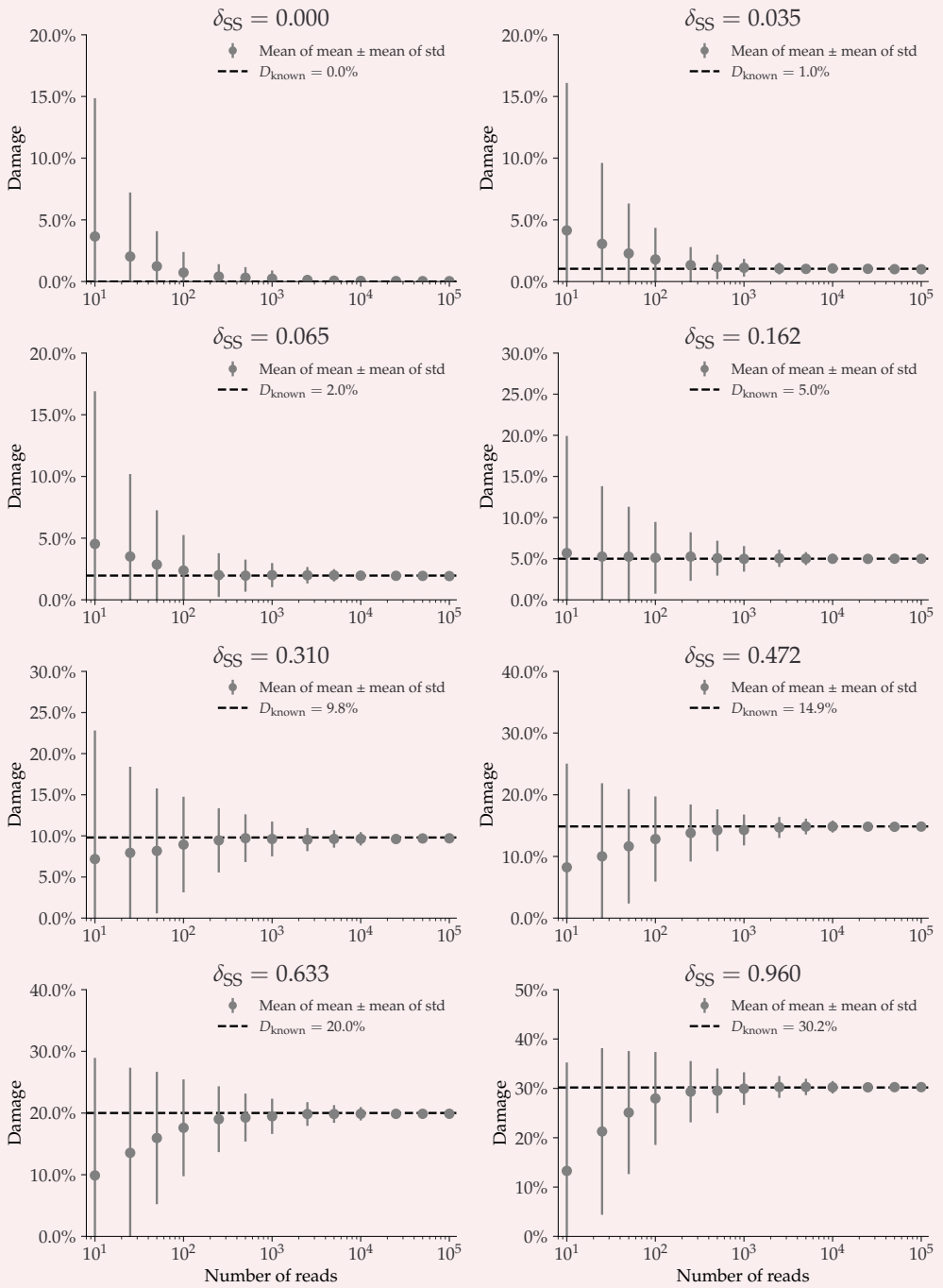
794

**Appendix 4—figure S12.** This plot shows the average damage as a function of the number of reads.

796

The grey points show the average of the individual means (with the average of the standard deviations as errors).

## Contig length: 1 000



798

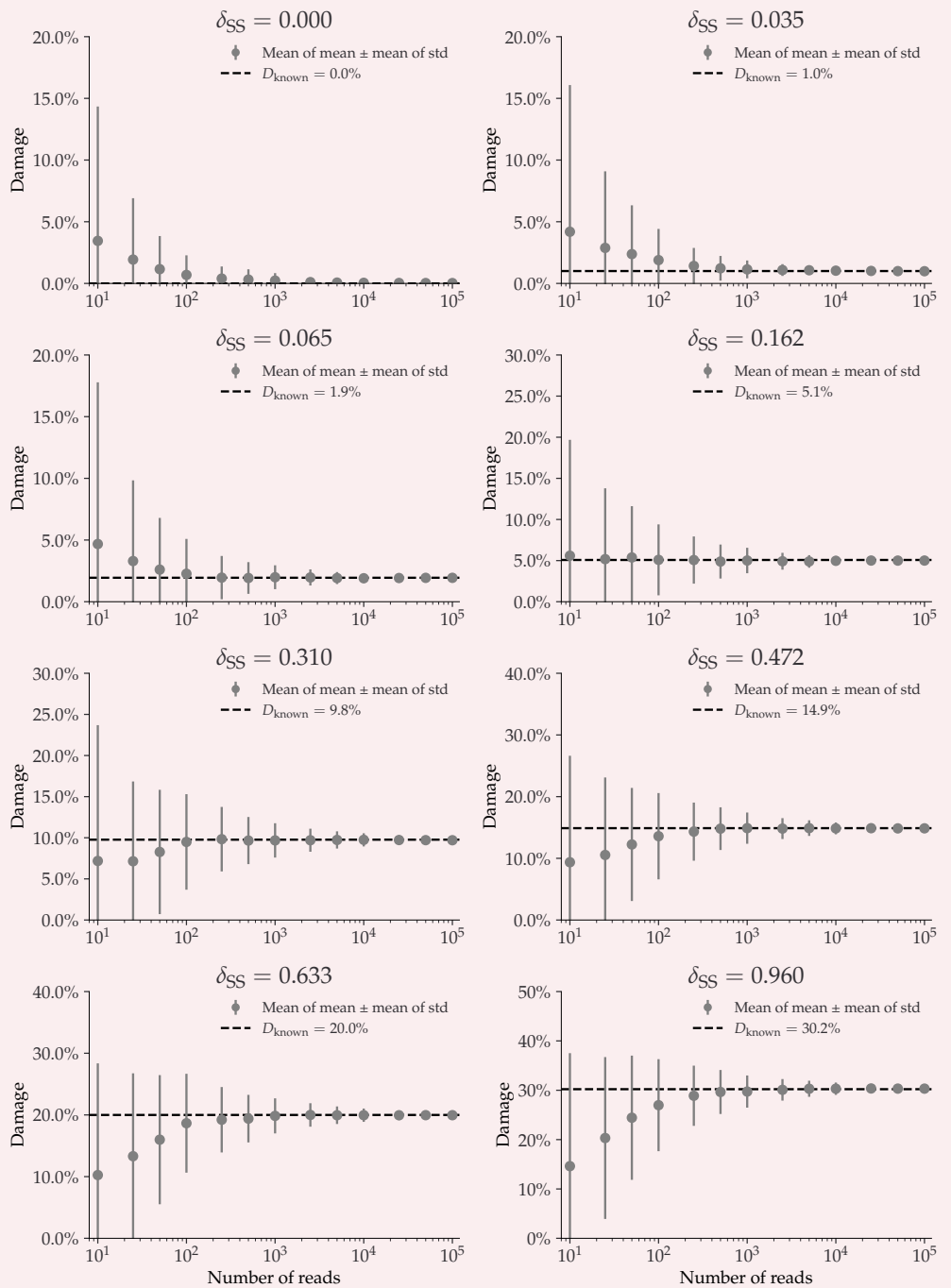
**Appendix 4—figure S13.** This plot shows the average damage as a function of the number of reads.

800

The grey points show the average of the individual means (with the average of the standard deviations as errors).

802

## Contig length: 10 000



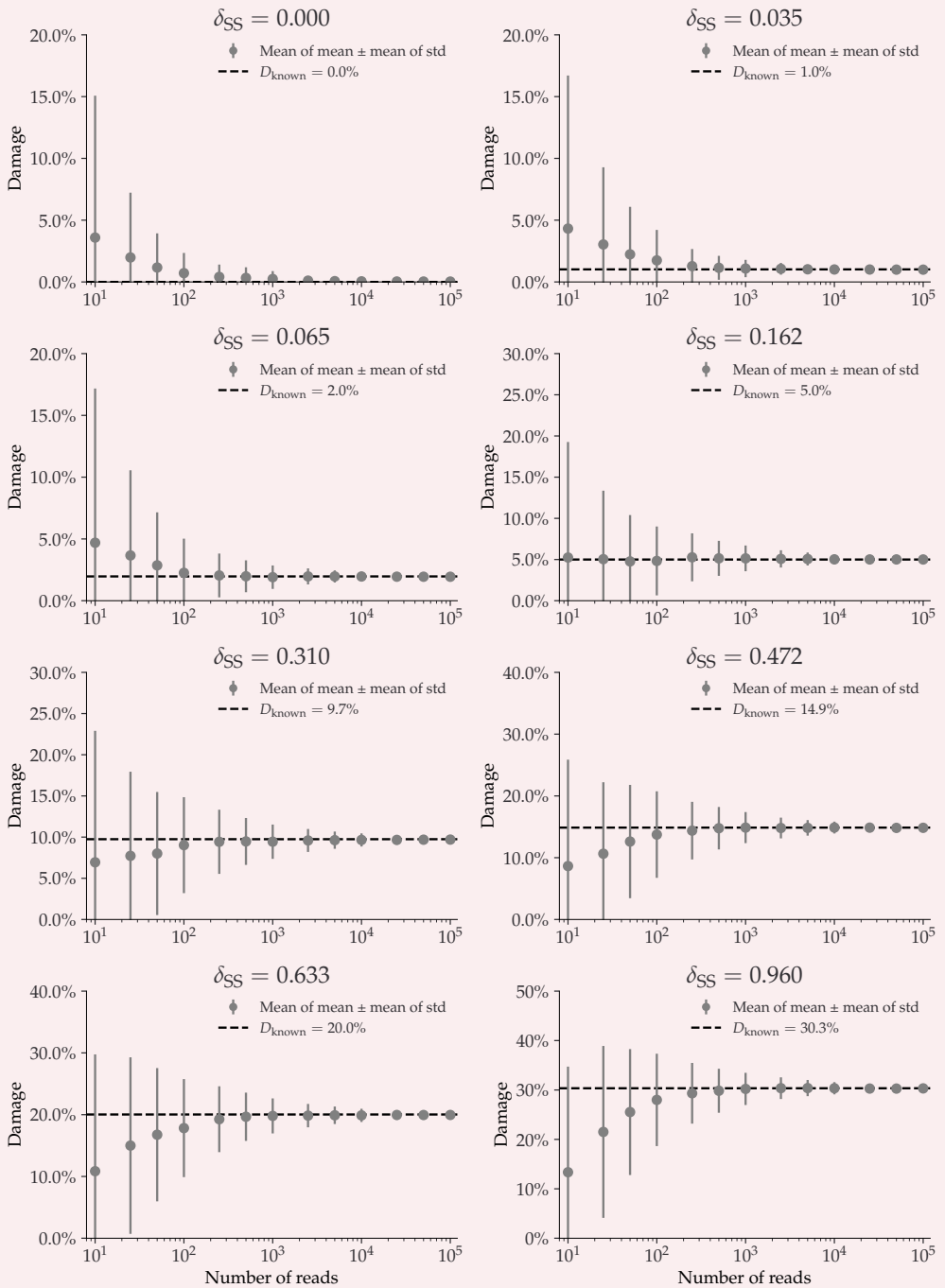
804

**Appendix 4—figure S14.** This plot shows the average damage as a function of the number of reads.

806

The grey points show the average of the individual means (with the average of the standard deviations as errors).

## Contig length: 100 000



808

**Appendix 4—figure S15.** This plot shows the average damage as a function of the number of reads.

810

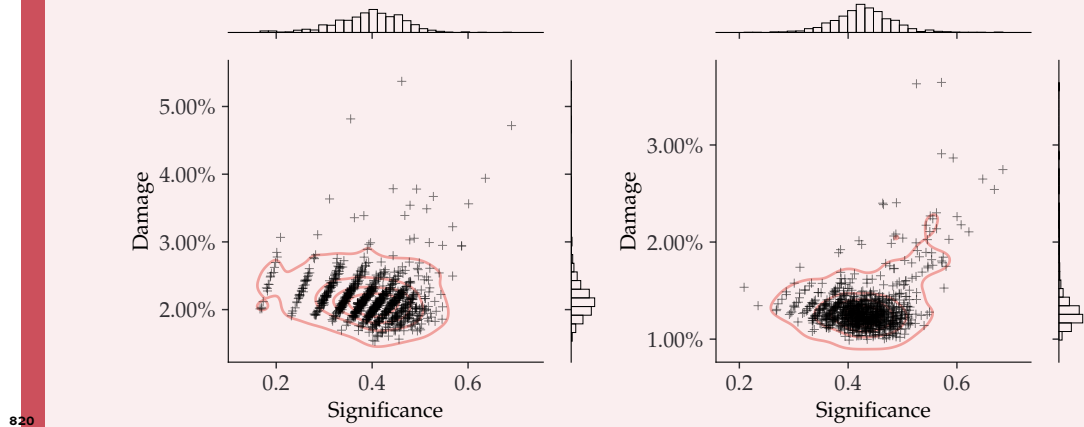
The grey points show the average of the individual means (with the average of the standard deviations as errors).

812

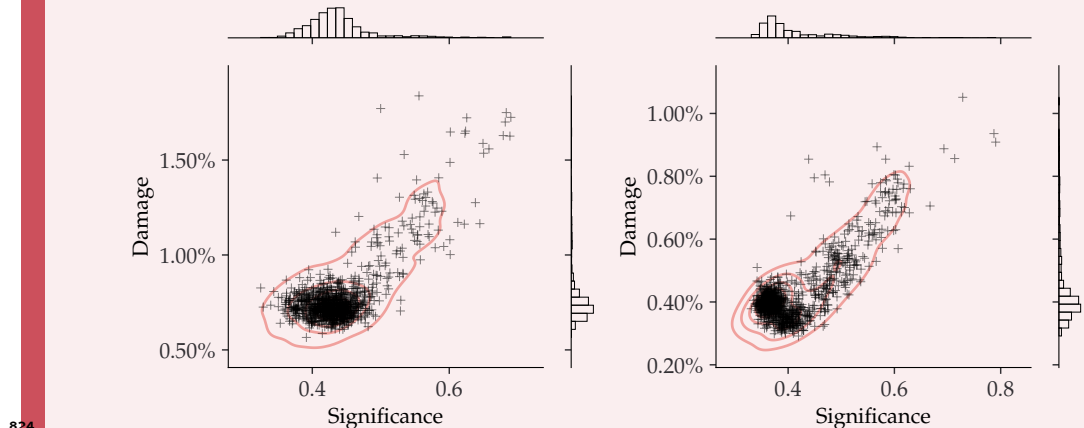
## Appendix 5

### NGSNGS SIMULATIONS – ZERO DAMAGE

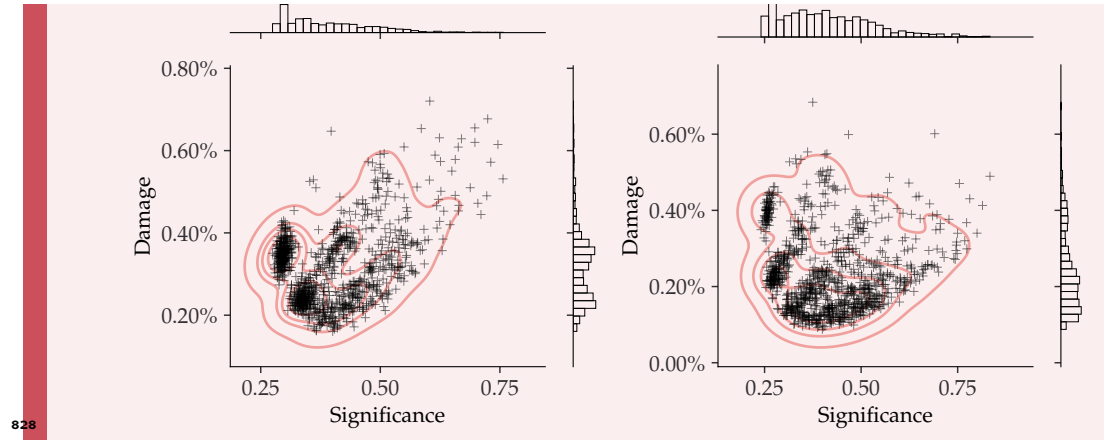
Damage estimates for non-damaged simulated data, each with 1000 replications, see [subsection 3.1](#). The inferred damage is shown on the y-axis and the significance on the x-axis. Each simulation is shown as a single cross and the red lines show the kernel density estimate (KDE) of the damage estimates. The marginal distributions are shown as histograms next to the scatter plot.



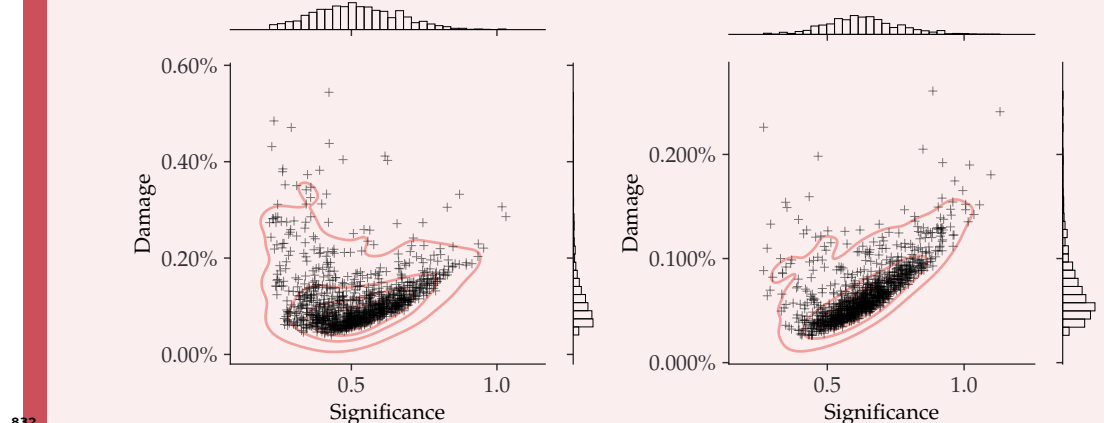
Appendix 5—figure S16. Left) 25 simulated reads. Right) 50 simulated reads.



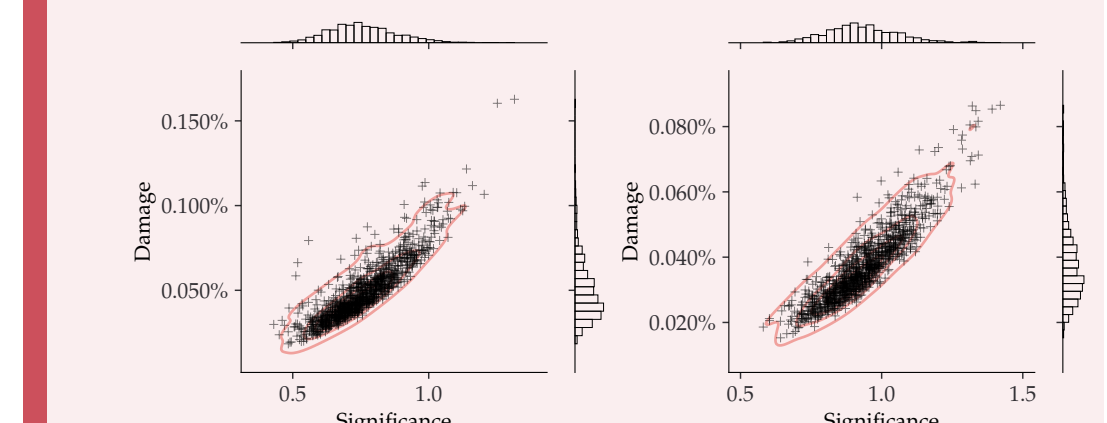
Appendix 5—figure S17. Left) 100 simulated reads. Right) 250 simulated reads.



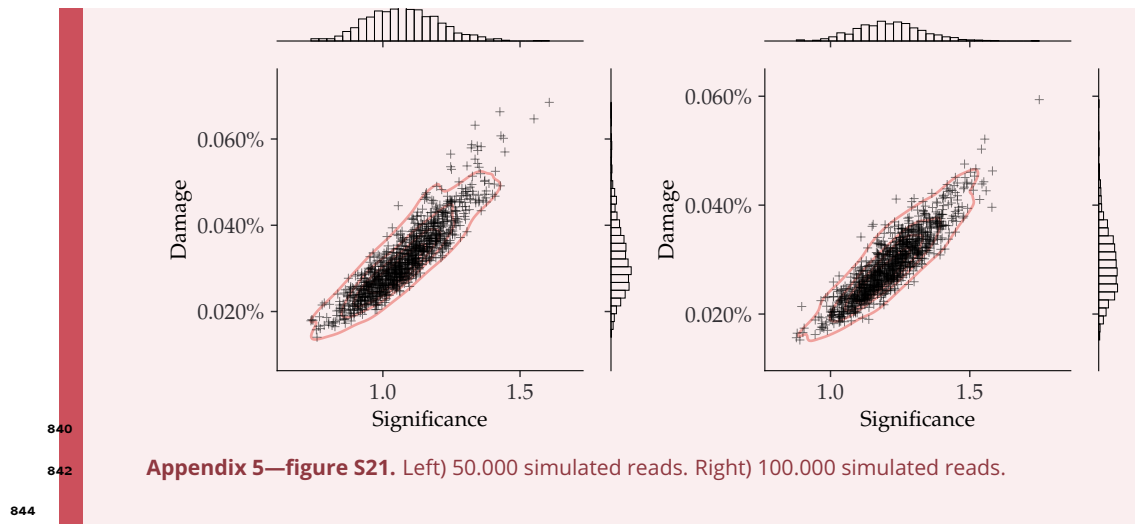
**Appendix 5—figure S18. Left) 500 simulated reads. Right) 1.000 simulated reads.**



**Appendix 5—figure S19. Left) 2.500 simulated reads. Right) 5.000 simulated reads.**



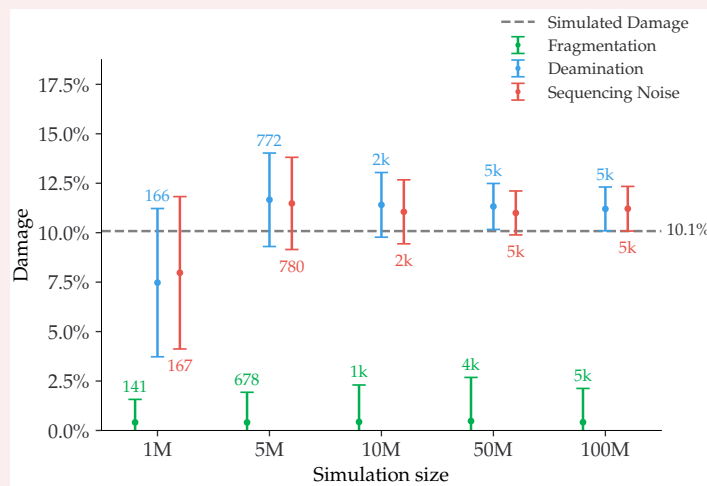
**Appendix 5—figure S20. Left) 10.000 simulated reads. Right) 25.000 simulated reads.**



## Appendix 6

### FALSE NEGATIVES

Even though the simple requirement of having more than 100 reads drastically improves the performance of the damage estimates, see [subsection 4.2](#), it does not identify all of the species that were simulated to be ancient. One of these non-identified taxa is the Stenotrophomonas Maltophilia species in the Pitch-6 sample. We show the damage estimates for different simulations for this particular taxa in [Figure S22](#) to quantify the behaviour of the damage estimate at the different stages of the simulation pipeline. For the final stage in the gargammel pipeline, ie. including fragmentation, deamination, and sequencing noise (red in the figure), only 167 reads are assigned to this specific taxa after mapping, when a total of 1 million reads were simulated. The significance is  $Z_{\text{fit}} = 1.9$ , just below the damage threshold.

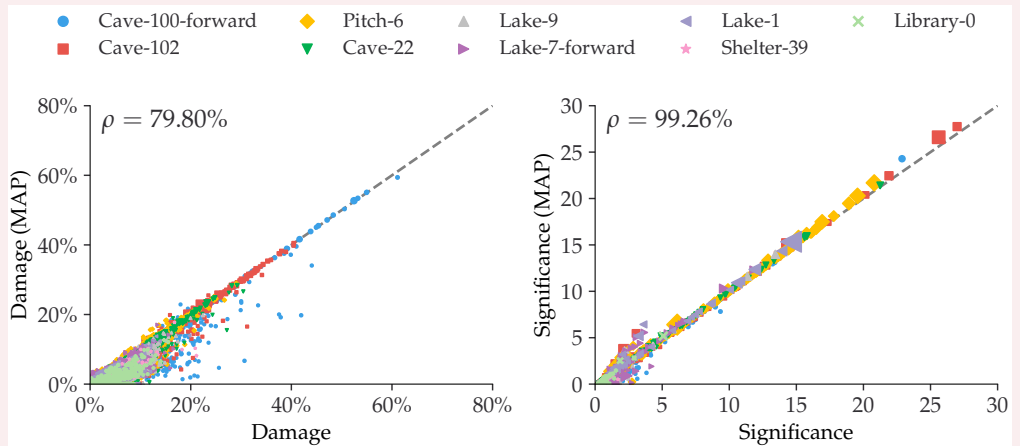


**Appendix 6—figure S22.** Damage estimates of the Stenotrophomonas maltophilia species from the Pitch-6 sample. Damage is shown as a function of the total simulation size, with the fragmentation files in green, the deamination files in blue and the final files including sequencing errors in red. All errors are  $1\sigma$  error bars (standard deviation). The number of reads for each fit is shown as text the simulated amount of damage is shown as a dashed grey line.

866

868

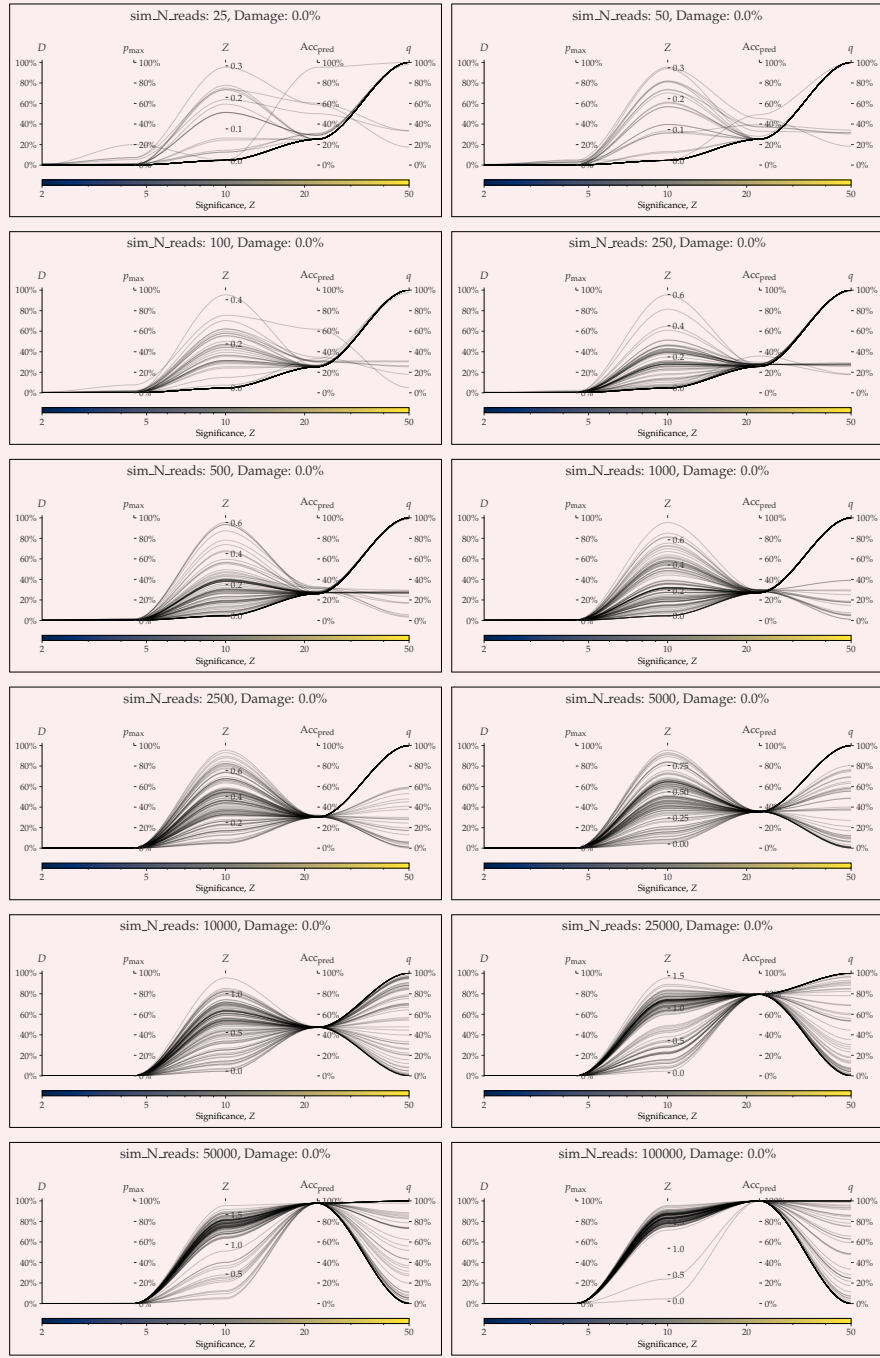
## BAYES VS. MAP



**Appendix 7—figure S23.** Comparison between the full Bayesian model and the fast, approximate, MAP model for the estimated damage and significance. The dashed, grey line shows the 1:1 ratio.

## PYDAMAGE COMPARISON

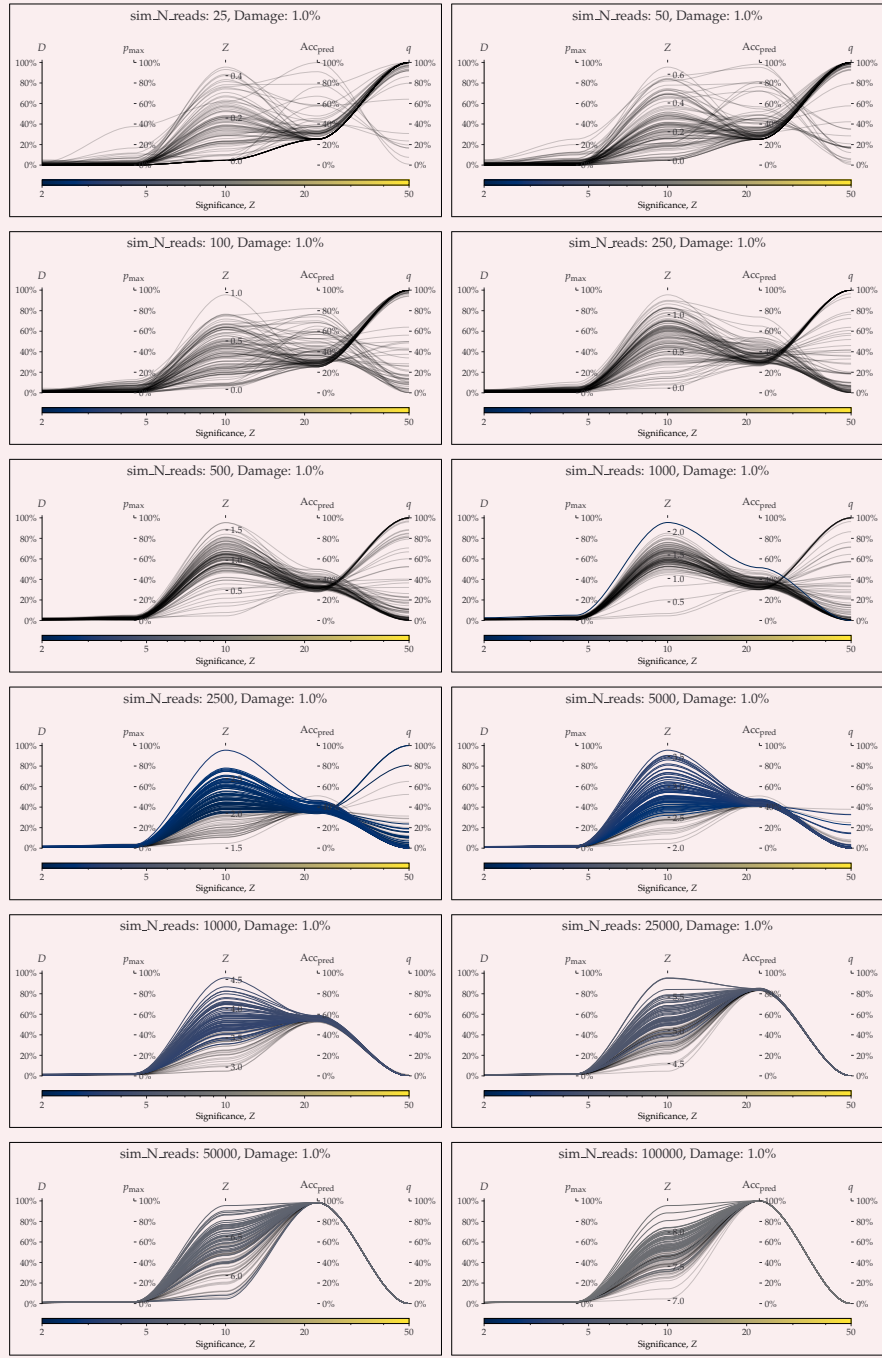
872 The following figures show the parallel coordinates plot comparing metaDMG and PyDamage  
873 for the Homo Sapiens single-genome simulation with 100 reads for different amount of ar-  
874 tificially added damage, see **subsection 4.5**. The two first axes show the estimated damage:  
875  $D_{\text{fit}}$  by metaDMG and  $p_{\text{max}}$  by PyDamage. The following two axes show the fit quality: signif-  
876 icance ( $Z_{\text{fit}}$ ) by metaDMG and the predicted accuracy ( $\text{Acc}_{\text{pred}}$ ) by PyDamage. The final axis  
877 shows the  $q$ -value by PyDamage. Each of the 100 replications are plotted as single lines.  
878 Replications passing the relaxed metaDMG damage threshold ( $D_{\text{fit}} > 1\%$  and  $Z_{\text{fit}} > 2$ ) are  
879 shown in color proportional to their significance. Replications that did not pass are shown  
880 in semi-transparent black lines.



882

884

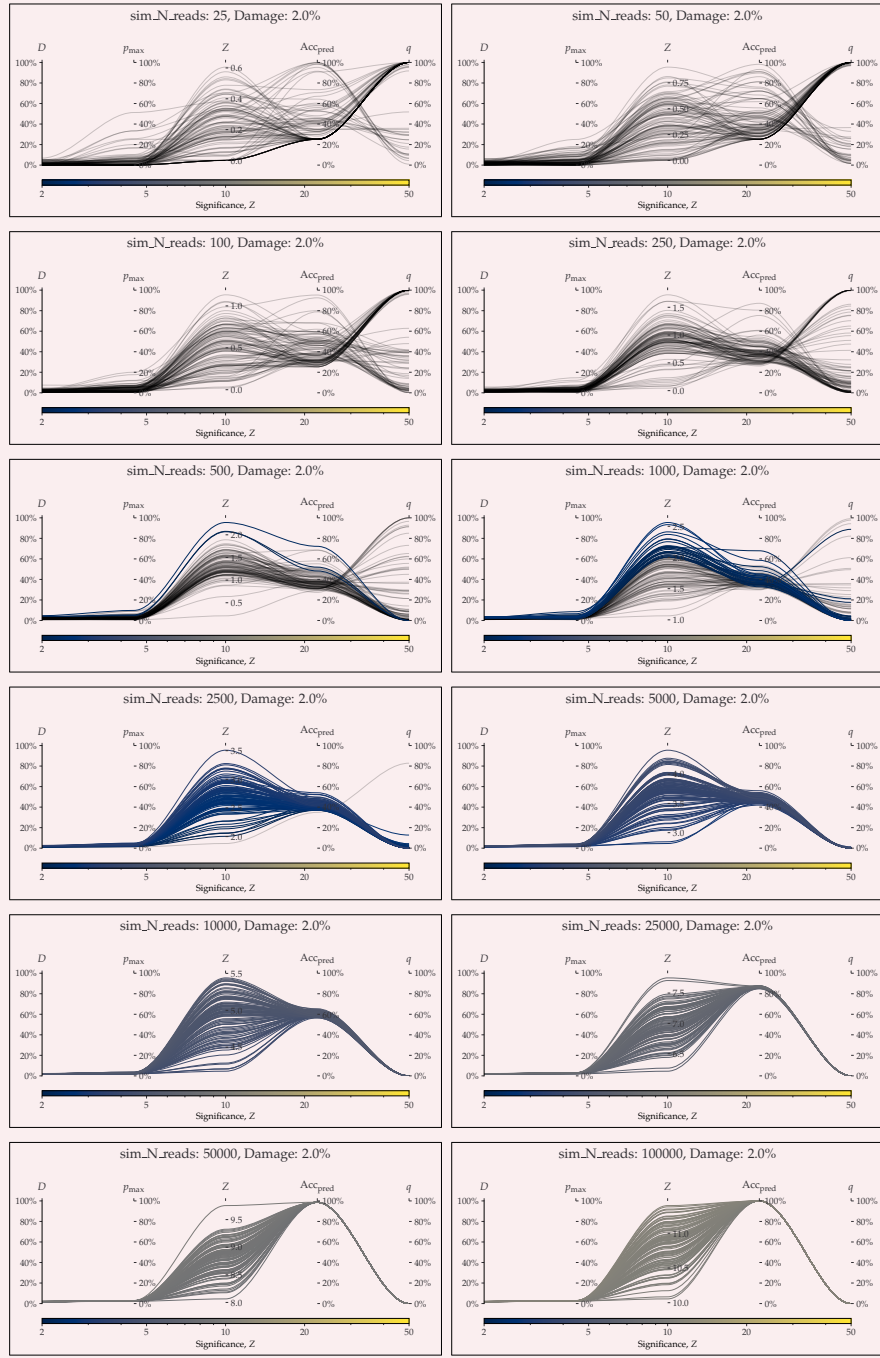
**Appendix 8—figure S24.** parallel coordinates plot comparing metaDMG and PyDamage for 0% artificial damage.



886

888

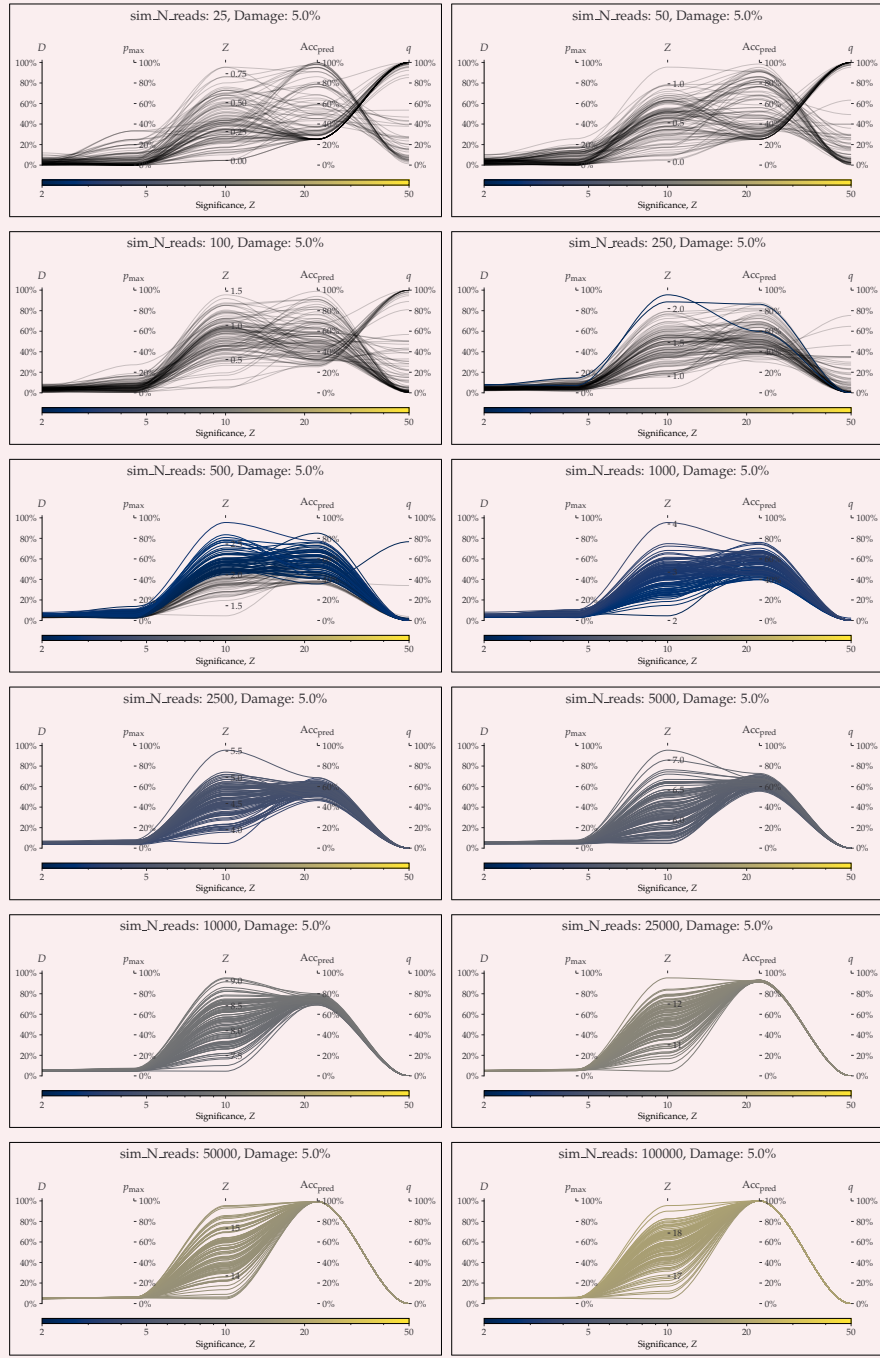
**Appendix 8—figure S25.** parallel coordinates plot comparing metaDMG and PyDamage for 1% artificial damage.



890

892

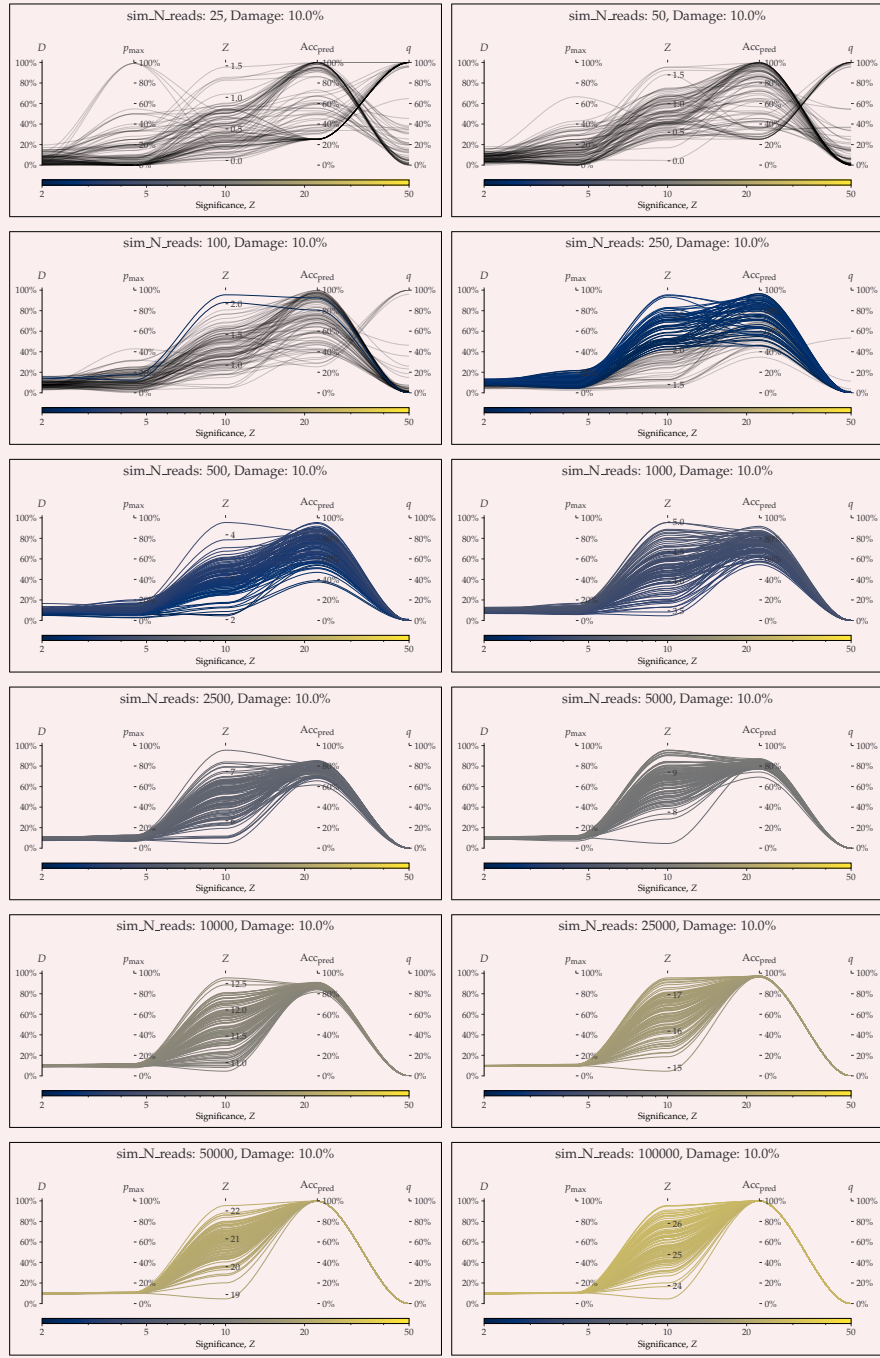
**Appendix 8—figure S26.** parallel coordinates plot comparing metaDMG and PyDamage for 2% artificial damage.



894

896

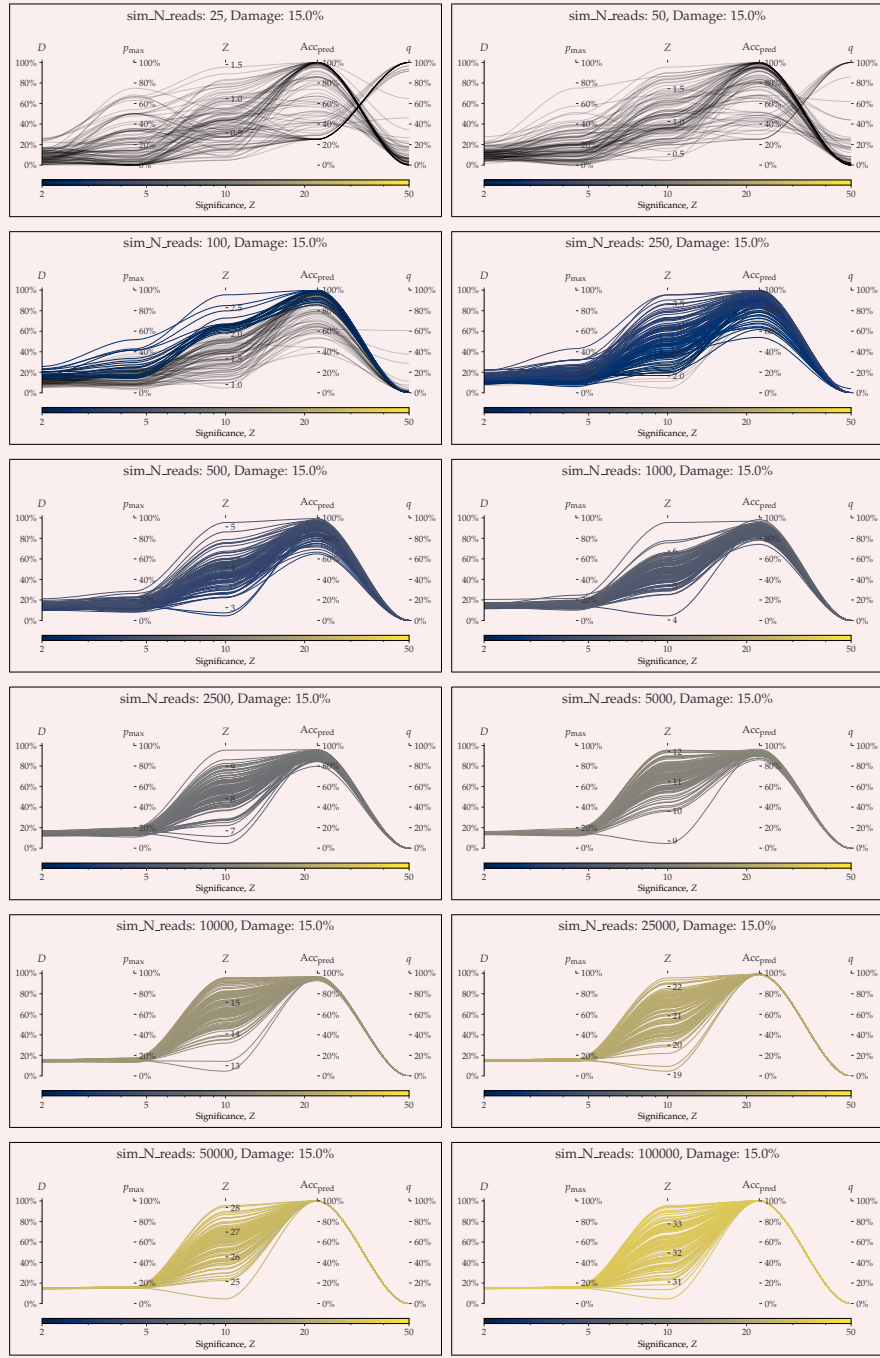
**Appendix 8—figure S27.** parallel coordinates plot comparing metaDMG and PyDamage for 5% artificial damage.



898

900

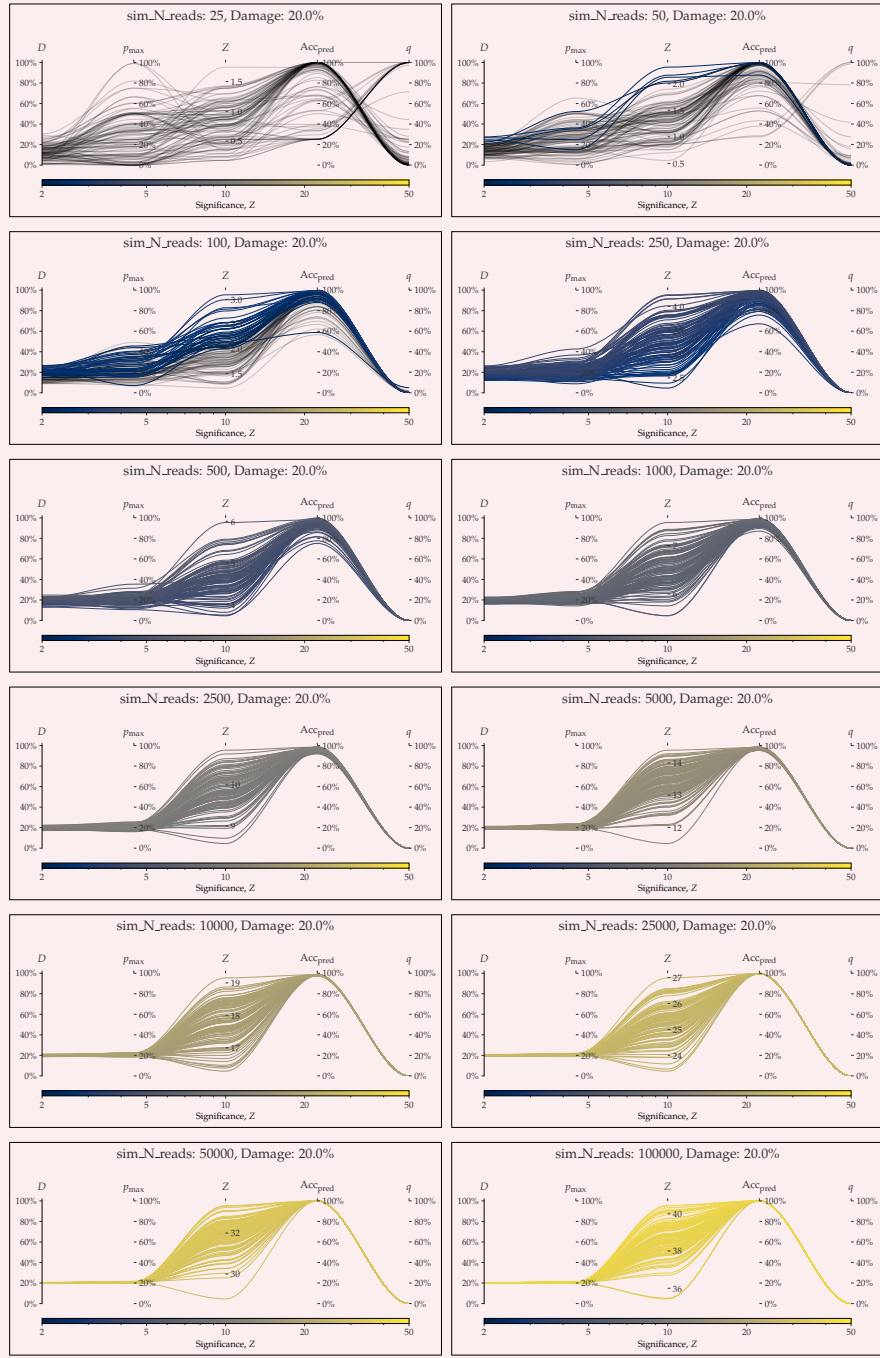
**Appendix 8—figure S28.** parallel coordinates plot comparing metaDMG and PyDamage for 10% artificial damage.



902

904

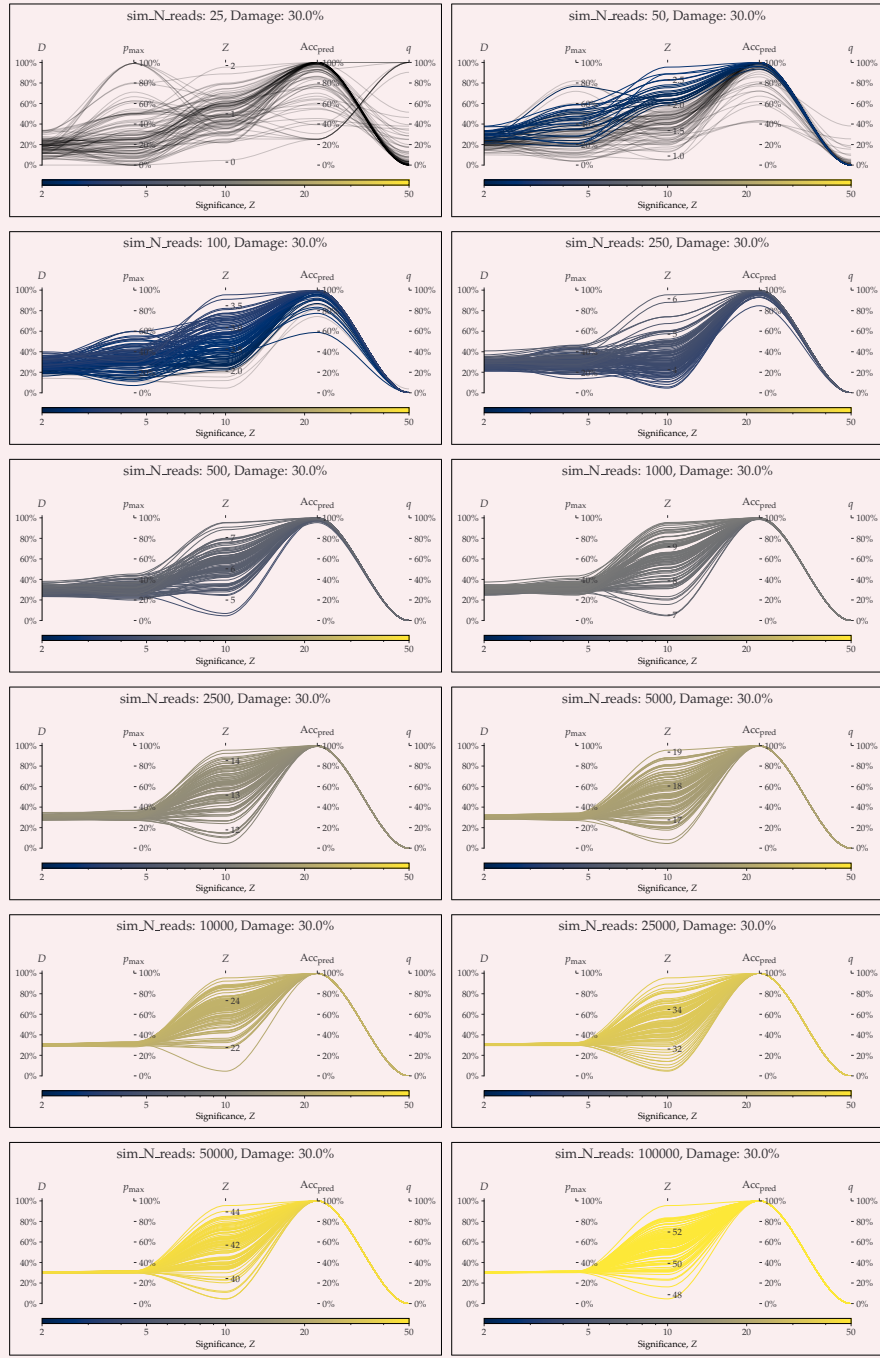
**Appendix 8—figure S29.** parallel coordinates plot comparing metaDMG and PyDamage for 15% artificial damage.



906

908

**Appendix 8—figure S30.** parallel coordinates plot comparing metaDMG and PyDamage for 20% artificial damage.



**910 Appendix 8—figure S31.** parallel coordinates plot comparing metaDMG and PyDamage for 30%  
**912** artificial damage.